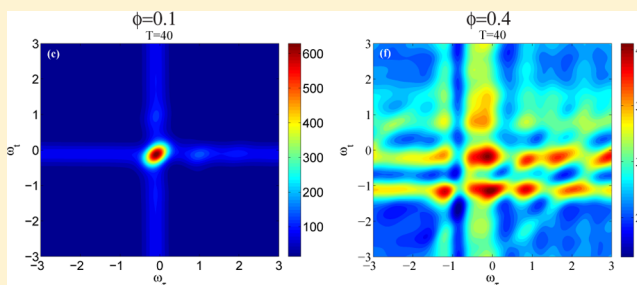


Fast, Accurate Simulation of Polaron Dynamics and Multidimensional Spectroscopy by Multiple Davydov Trial States

Nengji Zhou,^{†,‡} Lipeng Chen,[‡] Zhongkai Huang,[‡] Kewei Sun,[¶] Yoshitaka Tanimura,[§] and Yang Zhao^{*,‡}[†]Department of Physics, Hangzhou Normal University, Hangzhou 310046, China[‡]Division of Materials Science, Nanyang Technological University, Singapore 639798, Singapore[¶]School of Science, Hangzhou Dianzi University, Hangzhou 310046, China[§]Department of Chemistry, Graduate School of Science, Kyoto University, Kyoto 606-8502, Japan

ABSTRACT: By employing the Dirac–Frenkel time-dependent variational principle, we study the dynamical properties of the Holstein molecular crystal model with diagonal and off-diagonal exciton–phonon coupling. A linear combination of the Davydov D_1 (D_2) *ansatz*, referred to as the “multi- D_1 *ansatz*” (“multi- D_2 *ansatz*”), is used as the trial state with enhanced accuracy but without sacrificing efficiency. The time evolution of the exciton probability is found to be in perfect agreement with that of the hierarchy equations of motion, demonstrating the promise the multiple Davydov trial states hold as an efficient, robust description of dynamics of complex quantum systems. In addition to the linear absorption spectra computed for both diagonal and off-diagonal cases, for the first time, 2D spectra have been calculated for systems with off-diagonal exciton–phonon coupling by employing the multiple D_2 *ansatz* to compute the nonlinear response function, testifying to the great potential of the multiple D_2 *ansatz* for fast, accurate implementation of multidimensional spectroscopy. It is found that the signal exhibits a single peak for weak off-diagonal coupling, while a vibronic multipeak structure appears for strong off-diagonal coupling.



1. INTRODUCTION

Thanks to recent advances in ultrafast spectroscopy, femtosecond photoexcitation has become a major technique in probing elementary excitations, which brought about numerous studies on relaxation dynamics of photoexcited entities, for example, polarons in inorganic liquids and solids,^{1–3} charge carriers in topological insulators,^{4,5} trapped electrons and holes in the semiconductor nanoparticles,^{6–8} and electron–hole pairs in light-harvesting complexes of photosynthesis.^{9–13} Emerging technological capabilities to control femtosecond pulse durations and down-to-1-Hz bandwidth resolutions offer unprecedented windows on vibrational dynamics and excitation relaxation. For example, progress in femtosecond spectroscopy has enabled the observation of a coherent phonon wave packet oscillating along an adiabatic potential surface associated with a self-trapped exciton in a crystal with strong exciton–phonon interactions.¹⁴ Taking advantage of ultrashort pulse widths of recent lasers, the femtosecond dynamics of polaron formation and exciton–phonon dressing have been observed in pump–probe experiments.^{15–17} These experiments have revealed a complex interplay between a single exciton and its surrounding phonons under nonequilibrium conditions, while theoretical developments have not been kept in parallel. In particular, modeling of polaron dynamics have not received much-deserved attention over the last six decades.^{18,19}

From a theoretical point of view, capturing time-dependent polaron formation requires an in-depth understanding of the

combined dynamics of the particle and the phonons in its environment.²⁰ A simple Hamiltonian is that of the extended Holstein molecular crystal model^{21,22} with simultaneous diagonal and off-diagonal exciton–phonon coupling, as shown in Figure 1a, where the diagonal coupling represents a nontrivial dependence of the exciton site energies on the lattice coordinates, and the off-diagonal coupling, a nontrivial dependence of the exciton transfer integral on the lattice coordinates.^{23–27} A large body of literature exists on the study of the conventional form of the Holstein Hamiltonian with the diagonal coupling only.^{28,29} It seems fundamental to take into account simultaneously diagonal and off-diagonal coupling to characterize solid-state excimers^{24,25} as a variety of experimental and theoretical studies imply a strong dependence of electronic tunneling upon certain coordinated distortions of neighboring molecules in the formation of bound excited states. However, complete understanding of the off-diagonal coupling and out-of-equilibrium phenomena remains elusive. Early treatments of the off-diagonal coupling include the Munn–Silbey theory,^{26,27,30} which is based upon a perturbative approach with additional constraints on canonical transformation coefficients determined by a self-consistency equation. The global-local (GL) *ansatz*,^{31,32} formulated by Zhao and co-

Received: December 21, 2015

Revised: February 8, 2016

Published: February 12, 2016

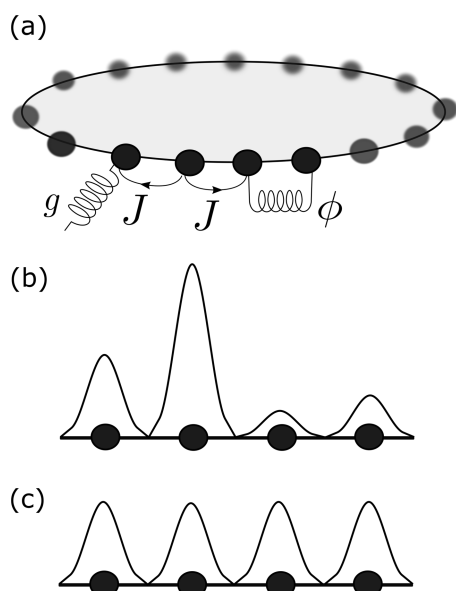


Figure 1. (a) Schematic of the Holstein ring. A simplified molecular crystal is treated as a ring where each point represent a two level molecule and the coils denote the phonons. (b and c) Phonon wave functions of the Davydov D_1 and D_2 *ansätze*, respectively. The phonon part of the D_1 *ansatz* depends on both sites and momentum, while that of the D_2 *ansatz* is site independent.

workers in the early 1990s, was subsequently employed in combination with the dynamic coherent potential approximation (with the Hartree approximation) to arrive at a state-of-the-art ground-state wave function as well as higher eigenstates.³³

Because an exact solution to the polaron dynamics still eludes us, several numerical approaches have been developed. For example, the time-dependent Schrödinger equation can be numerically integrated in real space for a few phonon time periods to probe the time evolution of electron and phonon densities and electron–phonon correlation functions.³⁴ However, the method is time-consuming and impractical when the size of the system is large. Fortunately, time-dependent variational approaches are still valid to treat the polaron dynamics in such cases as long as a proper trial wave function is adopted. Previously, static properties of the Holstein polaron and the spin-boson model were studied by Zhao and his co-workers with a set of trial wave functions based upon phonon coherent states, including the Toyozawa *ansatz*,^{31,35,36} the GL *ansatz*,^{31,32,36,37} a delocalized form of the Davydov D_1 *ansatz*,³⁸ and the multi- D_1 *ansatz*.³⁹ The results of these extended Davydov *ansätze* exhibit great promises in the investigation of the polaron energy band and other static properties of the Holstein polaron. However, difficulties surround accurate simulations of the polaron dynamics from an arbitrary initial state, such as a localized state for which the aforementioned Bloch states are not well suited. Thus, the question of what type of the variational trial state is suitable for the polaron dynamics of the Holstein model is still open.

By using the Dirac–Frenkel time-dependent variational principle, a powerful apparatus to reveal accurate dynamics of quantum many-body systems,⁴⁰ one can study the polaron dynamics of the Holstein model with simultaneous diagonal and off-diagonal exciton–phonon coupling. Time-dependent variational parameters, which specify the trial state, are obtained by solving a set of coupled differential equations generated

from the Lagrangian formalism of the Dirac–Frenkel variation. Validity of the trial states is carefully examined by quantifying how faithfully they follow the Schrödinger equation.^{28,29,41} The hierarchy of the Davydov *ansätze* includes two trial states of varying sophistication, referred to as the D_1 and D_2 *ansätze*,^{42–46} with the latter being a simplified version of the former. The D_1 *ansatz* is sufficient to describe the Holstein polaron dynamics with the diagonal coupling, but fails in the presence of the off-diagonal coupling. In comparison, the D_2 *ansatz* exhibits a nice dynamical performance with the off-diagonal coupling, though the deviation from the exact solution to the Schrödinger dynamics is not negligible.⁴¹ Instead, superposition of the D_1 or the D_2 *ansätze* will be adopted in our work, which offers significant improvements in the flexibility of the trial state,⁴⁷ thus yielding accurate polaron dynamics of the Holstein model with simultaneous diagonal and off-diagonal coupling.

Recently, two-dimensional (2D) electronic spectroscopy has been widely used to probe ultrafast energy transfer and charge separation processes in photosynthetic light harvesting complexes.^{48–54} Compared to linear spectroscopy techniques in which the spectral lines are often congested, ultrafast nonlinear spectroscopies can resolve dynamical processes with various time scales. In a 2D electronic spectroscopy experiment and apparatus, for example, three ultrashort laser pulses, separated by two time delays, namely, the coherence time and the waiting time, are incident on the sample, and the resultant signal field is spectrally resolved in a given phase-matched direction. The 2D contour plots of the signals provide direct information about excitonic relaxation and dephasing in a variety of molecular systems. Simulation of 2D electronic spectra of molecular aggregates was previously carried out for the Holstein model with the diagonal exciton–phonon coupling. However, the effect of off-diagonal coupling on the 2D spectra is yet to be addressed.

In this paper, the multiple Davydov trial states, called the multi- D_1 and multi- D_2 *ansätze*, will be adopted to simulate the polaron dynamics of an extended Holstein Hamiltonian that includes the off-diagonal exciton–phonon coupling. Validity of these trial states is carefully examined with the linear absorption spectra compared closely with the ground-state energy band. In addition, 2D spectra for systems with off-diagonal exciton–phonon coupling will be calculated by employing the multiple D_2 *ansatz*. The remainder of the paper is organized as follows. In section 2, we introduce the Holstein Hamiltonian and two novel variational wave functions on the basis of the multiple Davydov trial states, together with a criterion that quantifies the deviation of our trial states from the exact solution to the Schrödinger equation. In section 3, results are analyzed including the time evolution of the exciton amplitudes and the phonon displacements, the quantitative measurement for the trial state validity, and the linear absorption and 2D spectra. Finally, conclusions are drawn in section 4.

2. METHODOLOGY

2.1. Model. The Hamiltonian of the one-dimensional Holstein polaron is composed of

$$\hat{H} = \hat{H}_{\text{ex}} + \hat{H}_{\text{ph}} + \hat{H}_{\text{ex-ph}}^{\text{diag}} + \hat{H}_{\text{ex-ph}}^{\text{o.d.}} \quad (1)$$

where \hat{H}_{ex} , \hat{H}_{ph} , $\hat{H}_{\text{ex-ph}}^{\text{diag}}$, and $\hat{H}_{\text{ex-ph}}^{\text{o.d.}}$ represent the exciton Hamiltonian, the bath (phonon) Hamiltonian, the diagonal

exciton–phonon coupling Hamiltonian and the off-diagonal coupling Hamiltonian, respectively, which are defined as

$$\begin{aligned}\hat{H}_{\text{ex}} &= -J \sum_n \hat{a}_n^\dagger (\hat{a}_{n+1} + \hat{a}_{n-1}), \\ \hat{H}_{\text{ph}} &= \sum_q \omega_q \hat{b}_q^\dagger \hat{b}_q, \\ \hat{H}_{\text{ex-ph}}^{\text{diag}} &= -g \sum_{n,q} \omega_q \hat{a}_n^\dagger \hat{a}_n (e^{iqn} \hat{b}_q + e^{-iqn} \hat{b}_q^\dagger), \\ \hat{H}_{\text{ex-ph}}^{\text{o.d.}} &= \frac{1}{2} \phi \sum_{n,q} \omega_q \{ \hat{a}_n^\dagger \hat{a}_{n+1} [e^{iqn} (e^{iq} - 1) \hat{b}_q + \text{H. c.}] \\ &\quad + \hat{a}_n^\dagger \hat{a}_{n-1} [e^{iqn} (1 - e^{-iq}) \hat{b}_q + \text{H. c.}] \} \end{aligned} \quad (2)$$

where H.c. denotes the Hermitian conjugate, ω_q is the phonon frequency with momentum q , \hat{a}_n^\dagger (\hat{a}_n) is the exciton creation (annihilation) operator for the n th molecule, and \hat{b}_q^\dagger (\hat{b}_q) is the creation (annihilation) operator of a phonon with the momentum q ,

$$\hat{b}_q^\dagger = N^{-1/2} \sum_n e^{iqn} \hat{b}_n^\dagger, \quad \hat{b}_n^\dagger = N^{-1/2} \sum_q e^{-iqn} \hat{b}_q^\dagger \quad (3)$$

The parameters J , g and ϕ represent the transfer integral, diagonal and off-diagonal coupling strengths, respectively, and N is the number of sites in the Holstein ring. In this paper, a linear phonon dispersion is assumed

$$\omega_q = \omega_0 \left[1 + W \left(\frac{2|q|}{\pi} - 1 \right) \right] \quad (4)$$

where ω_0 denotes a central phonon frequency, W is the bandwidth falling between 0 and 1, and $q = 2\pi l/N$ represents the momentum index with $l = -\frac{N}{2} + 1, \dots, \frac{N}{2}$.

2.2. Multiple Davydov Trial States. In the past, two typical Davydov trial states, i.e., the D_1 and D_2 *ansätze*, were used to obtain the time evolution of the Holstein polaron following the Dirac–Frenkel variation scheme. The D_2 *ansatz* is a simplified version of the D_1 *ansatz*, since the phonon displacements of the D_1 (D_2) trial state is site-dependent (site-independent), as illustrated in Figure 1b,c. Multiple Davydov trial states with the multiplicity M are then introduced in this paper, which can be constructed as follows

$$\begin{aligned} |D_1^M(t)\rangle &= \sum_i^M \sum_n^N \psi_{i,n} |n\rangle |\lambda_{i,n}\rangle, \\ &= \sum_i^M \sum_n^N \psi_{i,n} \hat{a}_n^\dagger |0\rangle_{\text{ex}} \exp\left\{ \sum_q [\lambda_{inq} \hat{b}_q^\dagger - \lambda_{inq}^* \hat{b}_q] \right\} |0\rangle_{\text{ph}} \end{aligned} \quad (5)$$

and

$$\begin{aligned} |D_2^M(t)\rangle &= \sum_i^M \sum_n^N \psi_{i,n} |n\rangle |\lambda_i\rangle, \\ &= \sum_i^M \sum_n^N \psi_{i,n} \hat{a}_n^\dagger |0\rangle_{\text{ex}} \exp\left\{ \sum_q [\lambda_{iq} \hat{b}_q^\dagger - \lambda_{iq}^* \hat{b}_q] \right\} |0\rangle_{\text{ph}} \end{aligned} \quad (6)$$

where $\psi_{i,n}$ and λ_{inq} are related to the exciton probability and the phonon displacement, respectively, n represents the site index in the molecular ring, and i labels the coherent superposition state. If $M = 1$, both the $|D_1^M(t)\rangle$ and $|D_2^M(t)\rangle$ *ansätze* are reduced to the usual Davydov D_1 and D_2 trial states, respectively. The equations of motion for the variational parameters $\psi_{i,n}$ and λ_{inq} are then derived by adopting the Dirac–Frenkel variational principle,

$$\begin{aligned} \frac{d}{dt} \left(\frac{\partial L}{\partial \psi_{i,n}^*} \right) - \frac{\partial L}{\partial \psi_{i,n}} &= 0, \\ \frac{d}{dt} \left(\frac{\partial L}{\partial \lambda_{inq}^*} \right) - \frac{\partial L}{\partial \lambda_{inq}} &= 0 \end{aligned} \quad (7)$$

For the multi- D_1 *ansatz* defined in eq 5, the Lagrangian L_1 is given as

$$\begin{aligned} L_1 &= \langle D_1^M(t) | \frac{i\hbar}{2} \frac{\partial}{\partial t} - \hat{H} | D_1^M(t) \rangle \\ &= \frac{i\hbar}{2} \left[\langle D_1^M(t) | \frac{\partial}{\partial t} | D_1^M(t) \rangle - \langle D_1(t) | \frac{\partial}{\partial t} | D_1^M(t) \rangle \right] \\ &\quad - \langle D_1^M(t) | \hat{H} | D_1^M(t) \rangle, \end{aligned} \quad (8)$$

where the first term yields

$$\begin{aligned} &\langle D_1^M(t) | \frac{\partial}{\partial t} | D_1^M(t) \rangle - \langle D_1^M(t) | \frac{\partial}{\partial t} | D_1^M(t) \rangle \\ &= \sum_{i,j}^M \sum_n^N (\psi_{jn}^* \dot{\psi}_{in} - \dot{\psi}_{jn}^* \psi_{in}) S_{ji} \\ &\quad + \sum_{i,j}^M \sum_n^N \psi_{jn}^* \psi_{in} S_{ji} \sum_q \left[\frac{\dot{\lambda}_{jmq}^* \lambda_{inq} + \lambda_{jmq}^* \dot{\lambda}_{inq}}{2} \right. \\ &\quad \left. - \frac{\dot{\lambda}_{inq} \lambda_{inq}^* + \lambda_{inq} \dot{\lambda}_{inq}^*}{2} + \lambda_{jmq}^* \dot{\lambda}_{inq} - \lambda_{inq} \dot{\lambda}_{jmq}^* \right] \end{aligned} \quad (9)$$

and the second term is

$$\begin{aligned} &\langle D_1^M(t) | \hat{H} | D_1^M(t) \rangle \\ &= \langle D_1^M(t) | \hat{H}_{\text{ex}} | D_1^M(t) \rangle + \langle D_1^M(t) | \hat{H}_{\text{ph}} | D_1^M(t) \rangle \\ &\quad + \langle D_1^M(t) | \hat{H}_{\text{ex-ph}}^{\text{diag}} | D_1^M(t) \rangle + \langle D_1^M(t) | \hat{H}_{\text{ex-ph}}^{\text{o.d.}} | D_1^M(t) \rangle \end{aligned} \quad (10)$$

Detailed derivations of the equations of motion for the variational parameters are given in Appendix A.

Similarly, the equations of motion for the multi- D_2 *ansatz* can be derived using the Dirac–Frenkel variational principle in eq 7 with the Lagrangian L_2 defined as

$$\begin{aligned}
 L_2 &= \langle D_2^M(t) | \frac{i\hbar}{2} \frac{\partial}{\partial t} - \hat{H} | D_2^M(t) \rangle \\
 &= \frac{i\hbar}{2} \left[\langle D_2^M(t) | \frac{\partial}{\partial t} | D_2^M(t) \rangle - \langle D_2^M(t) | \frac{\partial}{\partial t} | D_2^M(t) \rangle \right] \\
 &\quad - \langle D_2^M(t) | \hat{H} | D_2^M(t) \rangle
 \end{aligned} \tag{11}$$

Assuming the trial wave function $|D_{1,2}^M(t)\rangle = |\Psi(t)\rangle$ at time t , we introduce a deviation vector $\vec{\delta}(t)$ to quantify the accuracy of the variational dynamics based on the multiple Davydov trial states

$$\begin{aligned}
 \vec{\delta}(t) &= \vec{\chi}(t) - \vec{\gamma}(t) \\
 &= \frac{\partial}{\partial t} |\Psi(t)\rangle - \frac{\partial}{\partial t} |D_{1,2}^M(t)\rangle
 \end{aligned} \tag{12}$$

where the vectors $\vec{\chi}(t)$ and $\vec{\gamma}(t)$ obey the Schrödinger equation $\vec{\chi}(t) = \partial|\Psi(t)\rangle/\partial t = \frac{1}{i\hbar}\hat{H}|\Psi(t)\rangle$ and the Dirac–Frenkel variational dynamics $\vec{\gamma}(t) = \partial|D_{1,2}^M(t)\rangle/\partial t$ in eq 7, respectively. Using the Schrödinger equation and the relationship $|\Psi(t)\rangle = |D_{1,2}^M(t)\rangle$, the deviation vector $\vec{\delta}(t)$ can be calculated as

$$\vec{\delta}(t) = \frac{1}{i\hbar} \hat{H} |D_{1,2}^M(t)\rangle - \frac{\partial}{\partial t} |D_{1,2}^M(t)\rangle \tag{13}$$

Thus, deviation from the exact Schrödinger dynamics can be indicated by the amplitude of the deviation vector $\Delta(t) = \|\vec{\delta}(t)\|$. In order to view the deviation in the parameter space (W, J, g, ϕ) , a dimensionless relative deviation σ is calculated as

$$\sigma = \frac{\max\{\Delta(t)\}}{\text{mean}\{N_{\text{err}}(t)\}}, t \in [0, t_{\text{max}}] \tag{14}$$

where $N_{\text{err}}(t) = \|\vec{\chi}(t)\|$ is the amplitude of the time derivative of the wave function,

$$\begin{aligned}
 N_{\text{err}}(t) &= \sqrt{\langle \frac{\partial}{\partial t} \Psi(t) | \frac{\partial}{\partial t} \Psi(t) \rangle} \\
 &= \sqrt{\langle D_{1,2}^M(t) | \hat{H}^2 | D_{1,2}^M(t) \rangle} \\
 &\approx \Delta E
 \end{aligned} \tag{15}$$

since $\langle E \rangle = \langle D_{1,2}^M(t) | \hat{H} | D_{1,2}^M(t) \rangle \approx 0$ in this paper.

Two types of initial states are considered, i.e., the exciton either sits on a single site for diagonal coupling cases or on two nearest-neighboring sites for off-diagonal coupling cases. Other initial states, such as Gaussian and uniform distributions for the exciton occupation, have also been investigated, leading to similar results but with larger relative errors. To avoid singularity, noise satisfying the uniform distribution $[-10^{-5}, 10^{-5}]$ is added to the variational parameters $\psi_{i,n}$ and $\lambda_{i,q}$ ($\lambda_{i,q}$) of the initial states. With the wave functions $|D_1^M(t)\rangle$ and $|D_2^M(t)\rangle$ at hand, the energy of the Holstein polaron $E_{\text{total}} = E_{\text{ex}} + E_{\text{ph}} + E_{\text{diag}} + E_{\text{off}}$ is calculated, where $E_{\text{ex}} = \langle D_{1,2}^M | \hat{H}_{\text{ex}} | D_{1,2}^M \rangle$, $E_{\text{ph}} = \langle D_{1,2}^M | \hat{H}_{\text{ph}} | D_{1,2}^M \rangle$, $E_{\text{diag}} = \langle D_{1,2}^M | \hat{H}_{\text{ex-ph}}^{\text{diag}} | D_{1,2}^M \rangle$ and $E_{\text{off}} = \langle D_{1,2}^M | \hat{H}_{\text{ex-ph}}^{\text{o.d.}} | D_{1,2}^M \rangle$. In addition, the exciton probability $P_{\text{ex}}(t, n)$ and the phonon displacement $X_{\text{ph}}(t, n)$ are defined as follows

$$\begin{aligned}
 P_{\text{ex}}(t, n) &= \langle D_{1,2}^M | \hat{a}_n^\dagger \hat{a}_n | D_{1,2}^M \rangle, \\
 X_{\text{ph}}(t, n) &= \langle D_{1,2}^M | \hat{b}_n + \hat{b}_n^\dagger | D_{1,2}^M \rangle
 \end{aligned} \tag{16}$$

Optical spectroscopy is another important aspect for the investigation of the polaron dynamics, as it provides valuable information on various correlation functions. First of all, the linear absorption spectra $F(\omega)$ calculated from the polaron dynamics on the basis of different *ansätze* will be comprehensively studied. The autocorrelation function $F(t)$ of the exciton–phonon system is introduced

$$\begin{aligned}
 F(t) &= {}_{\text{ph}} \langle \langle 0 |_{\text{ex}} 0 | e^{i\hat{H}t} \hat{P} e^{-i\hat{H}t} \hat{P}^\dagger | 0 \rangle_{\text{ex}} | 0 \rangle_{\text{ph}} \\
 &= {}_{\text{ph}} \langle \langle 0 |_{\text{ex}} \langle 0 | \hat{P} e^{-i\hat{H}t} \hat{P}^\dagger | 0 \rangle_{\text{ex}} | 0 \rangle_{\text{ph}}
 \end{aligned} \tag{17}$$

with the polarization operator

$$\hat{P} = \mu \sum_n (\hat{a}_n^\dagger | 0 \rangle_{\text{ex}} \langle 0 | + | 0 \rangle_{\text{ex}} \langle 0 | \hat{a}_n) \tag{18}$$

The linear absorption $F(\omega)$ is then calculated by means of the Fourier transformation,

$$F(\omega) = \frac{1}{\pi} \text{Re} \int_0^\infty F(t) e^{i\omega t} dt \tag{19}$$

In addition to the information provided by the linear absorption spectra, 2D electronic spectra provide direct knowledge on coupling between different exciton states and dephasing and relaxation processes that are elusive in the output from the traditional 1D spectroscopy. Theoretical simulation of 2D spectra involves the calculation of third order polarization $P(t)$, which can be expressed in terms of the nonlinear response functions R_i , where i goes from 1 to 4.^{55–57} The 2D electronic spectra are measured in two configurations that correspond to the rephasing (subscript R) and non-rephasing (subscript NR) contribution to the third order polarization $P(t)$, which, in the impulsive approximation, can be written as

$$\begin{aligned}
 P_R^{(3)}(t, T, \tau) &\sim -i[R_2(t, T, \tau) + R_3(t, T, \tau)], \\
 P_{NR}^{(3)}(t, T, \tau) &\sim -i[R_1(t, T, \tau) + R_4(t, T, \tau)]
 \end{aligned} \tag{20}$$

where τ (the so-called coherence time) is the delay time between the first and second pulses, T (the so-called population time) is the delay time between the second and third pulses, and t is the delay time between the third pulse and measured signal. The rephasing and nonrephasing 2D spectra can be then obtained by performing 2D Fourier–Laplace transformation of eq 20 as follows

$$\begin{aligned}
 S_R(\omega_t, T, \omega_\tau) &= \text{Re} \int_0^\infty \int_0^\infty dt d\tau i P_R^{(3)}(t, T, \tau) e^{-i\omega_\tau \tau + i\omega_t t}, \\
 S_{NR}(\omega_t, T, \omega_\tau) &= \text{Re} \int_0^\infty \int_0^\infty dt d\tau i P_{NR}^{(3)}(t, T, \tau) e^{i\omega_\tau \tau + i\omega_t t}
 \end{aligned} \tag{21}$$

The total 2D signal is defined as the sum of the nonrephasing and the rephasing part

$$S(\omega_t, T, \omega_\tau) = S_R(\omega_t, T, \omega_\tau) + S_{NR}(\omega_t, T, \omega_\tau) \tag{22}$$

In this work, we will apply the multiple D_2 states to calculate the nonlinear response functions R_i with special attention paid to the role of the off-diagonal exciton–phonon coupling on the 2D spectra. The reader is referred to the Appendix D for more details on the applications of the multiple D_2 *ansätze* to the simulation of 2D spectra.

3. NUMERICAL RESULTS

3.1. Validity of Variational Dynamics. Figure 2 illustrates the time evolution of the system energies, including the exciton

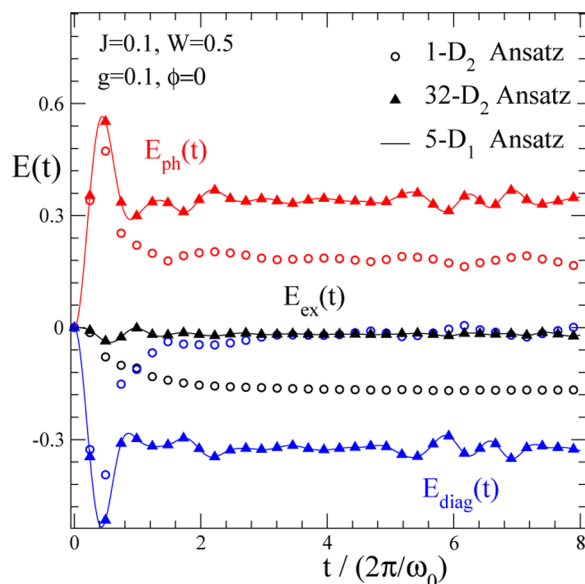


Figure 2. Energies of the exciton, the phonons, and the exciton–phonon interaction, i.e., $E_{\text{ex}}(t)$, $E_{\text{ph}}(t)$, and $E_{\text{diag}}(t)$, are displayed as a function of the time t for the weak coupling case of $J = 0.1$, $g = 0.1$, $W = 0.5$, and $\phi = 0$. The open circles, the solid triangles and the solid line correspond to the results obtained with the single D_2 , $D_2^{M=32}$, and $D_1^{M=5}$ ansätze, respectively.

energy E_{ex} , the phonon energy E_{ph} and the exciton–phonon interaction energy E_{diag} for a diagonal coupling only case with transfer integral $J = 0.1$, bandwidth $W = 0.5$ and coupling strength $g = 0.1$. For a molecular ring of 16 sites, the energies obtained with three different ansätze are compared (the open circles, the solid triangles and the solid line correspond to the single D_2 , $D_2^{M=32}$, $D_1^{M=5}$ ansatz, respectively). Results obtained with the multi- D_2 ansatz with $M = 32$ display obvious deviations from those by the single D_2 ansatz, demonstrating the improvement produced by the multiple Davydov trial states over its single ansatz counterpart. In addition, the dynamics generated on the D_1 trial state can be made more accurate by the $D_1^{M=5}$ ansatz, and results of E_{ex} , E_{ph} and E_{diag} by the $D_1^{M=5}$ ansatz are in perfect agreement with those obtained with the $D_2^{M=32}$ ansatz, which indicates the robustness of the polaron dynamics based on the multiple Davydov trial states when the multiplicity M is sufficiently large.

A comprehensive test of the validity for our new trial states consisting of the multiple Davydov ansätze is performed for various parameters sets (J, W, g, ϕ). In Figure 3a, the relative deviation σ , given by eq 14, is displayed as a function of $1/M$, for the diagonal coupling case of $J = 0.1$, $W = 0.5$, $g = 0.1$ and $\phi = 0$. As M increases, the relative error σ monotonically decreases, and the value $\sigma = 0.067$ obtained at $1/M = 0.2$ is very small, which indicates the length of the deviation vector $\delta(t)$, as defined in eq 12, is negligibly small with respect to those of the vectors $\vec{\chi}(t)$ and $\vec{\gamma}(t)$. Moreover, the result that the deviation obtained by the $D_1^{M=5}$ ansatz is comparable with $\sigma = 0.033$ obtained with the $D_2^{M=32}$ ansatz demonstrates the accuracy of the multiple Davydov trial states when M is sufficiently large.

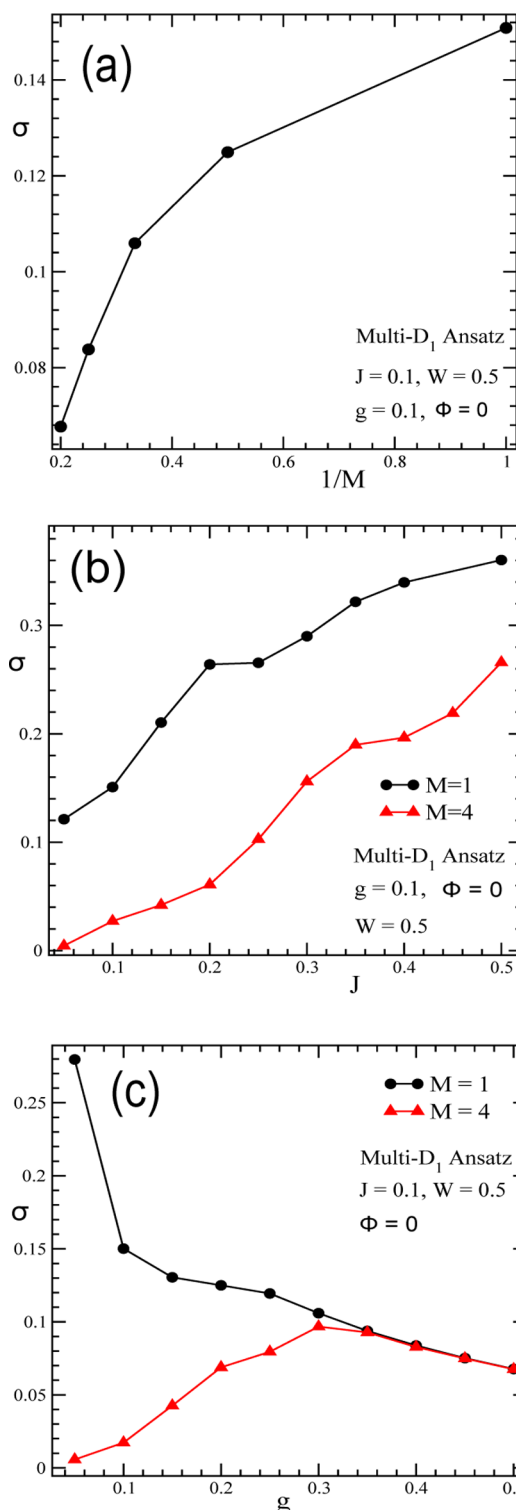


Figure 3. (a) Relative deviation σ of the multi- D_1 ansatz in a 16-site molecular ring is displayed as a function of $1/M$. The set of parameters $J = 0.1$, $g = 1$, $W = 0.5$, and $\phi = 0$ is used. Moreover, the relative deviation σ for the diagonal coupling case is also plotted as a function of the transfer integral J in part b and diagonal coupling strength g in part c. For both cases, the lines with circles and triangles correspond to the results obtained with the multiplicity $M = 1$ and $M = 4$, respectively.

In Figure 3b, the relative deviation σ is displayed as a function of the transfer integral J with circles and triangles

corresponding to results obtained by the multi- D_1 ansätze with $M = 1$ and 4, respectively. Other parameters used in the simulation are $g = 0.1$, $W = 0.5$ and $\phi = 0$. An obvious reduction in the relative error σ has been found when the multiplicity M is increased for the entire J regime. Similarly, the relative error σ against the diagonal coupling strength g is displayed in Figure 3c for $M = 1$ and 4, respectively. The relative error σ is obviously reduced for the multiplicity $M = 4$ in comparison with that for $M = 1$ when $g < 0.3$. However, these two curves overlap for $g > 0.3$ as the exciton is self-trapped in one of the sites. The above results indicate that the multiple Davydov trial states will significantly improve the accuracy of the delocalized state, while in the localized state the single D_1 ansatz is sufficient. In addition, the multiple Davydov trial states in the off-diagonal coupling case are also investigated with the nonzero value of ϕ . Taking the set of parameters $\phi = 0.4$ and $g = J = W = 0$ as an example, the relative error σ is displayed as a function of $1/M$ in Figure 4. As M increases, the

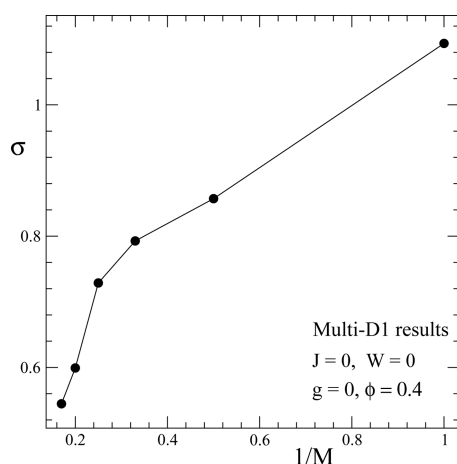


Figure 4. Relative deviation σ from the multi- D_1 ansatz is displayed as a function of $1/M$ for the off-diagonal coupling case with the coupling strength $\phi = 0.4$, and other parameters $J = W = g = 0$ are set.

relative error σ decreases, similar to the diagonal coupling case as shown in Figure 3a, although the value of σ for $M = 6$ ($\sigma = 0.54$) remains relatively large. For off-diagonal coupling, considerable improvements in accuracy can be achieved by utilizing multi- D_2 with the increase of multiplicity M (see discussions in ref 47).

3.2. Exciton Probabilities and Phonon Displacements.

Dynamical properties of the Holstein polaron, including the exciton probabilities and phonon displacements, are investigated by using the multiple Davydov trial states, and in comparison with those obtained with the single Davydov ansatz and the numerically exact HEOM method^{58–61} (see Appendix B). Figure 5 illustrates the time evolution of the exciton probability $P_{\text{ex}}(t, n)$ for the case of $J = 0.5$, $W = 0.5$, $g = 0.1$ and $\phi = 0$. For simplicity, a small ring with $N = 10$ sites is used in the simulations. As depicted in Figure 5a,b, distinguishable deviation in $P_{\text{ex}}(t, n)$ can be found between the variational results from the $D_1^{M=1}$ and $D_1^{M=8}$ ansätze. Interestingly, the exciton probability $P_{\text{ex}}(t, n)$ obtained from the HEOM method almost overlaps with that obtained by the $D_1^{M=8}$ ansatz (see Figure 5b,c). Furthermore, the exciton probability difference between the variational method and the HEOM method, $\Delta P_{\text{ex}}(t, n)$, as depicted in Figure 5d, is two orders of magnitude smaller than the value of $P_{\text{ex}}(t, n)$. It indicates that the

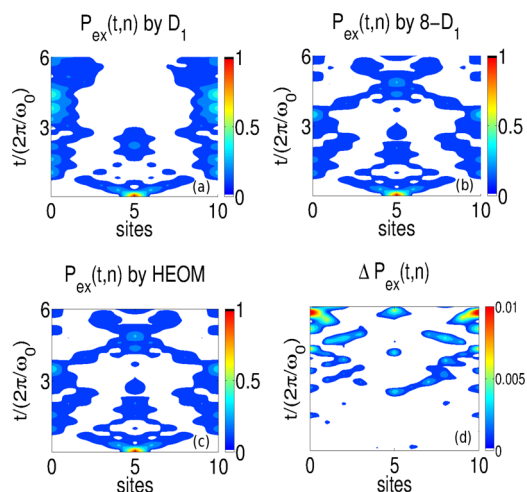


Figure 5. Time evolution of the exciton probability $P_{\text{ex}}(t, n)$ for the case of $J = 0.5$, $W = 0.5$, $g = 0.1$ and $\phi = 0$ is displayed in parts a–c, corresponding to the results obtained with the single D_1 ansatz, the $D_1^{M=8}$ ansatz and the HEOM method, respectively. The difference $\Delta P_{\text{ex}}(t, n)$ between the HEOM and the $D_1^{M=8}$ variational method is also displayed in part d. We set the size of the molecular ring $N = 10$ in simulations.

variational dynamics of the Holstein polaron can be numerically exact if the multiplicity M of the D_1 ansatz is sufficiently large. In Figure 6, the exciton probabilities $P_{\text{ex}}(t, n)$ at the site $n = 5$

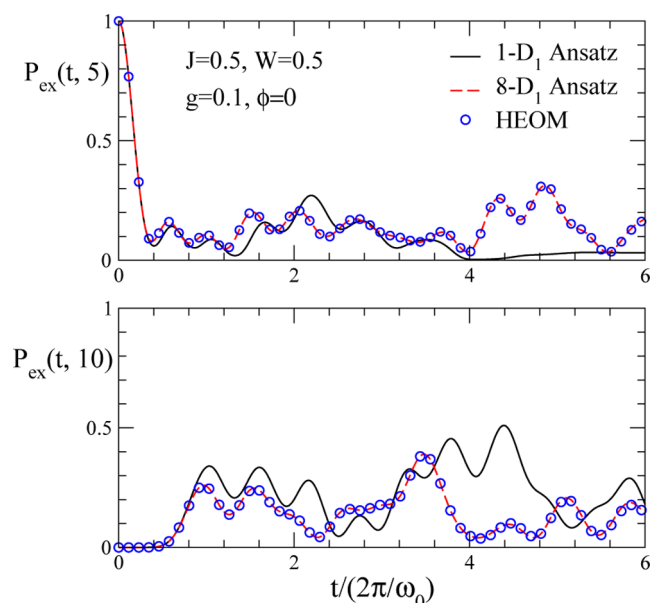


Figure 6. Time evolution of the exciton probability $P_{\text{ex}}(t, n)$ at $n = 5$ and 10 are displayed in the top and bottom panel for the case of $J = 0.5$, $W = 0.5$, $g = 0.1$ and $\phi = 0$. In each panel, the solid line, the dashed lines and the circles correspond to the variational results obtained with the single D_1 and $D_1^{M=8}$ ansätze and the HEOM results, respectively. The size of the molecular ring is set to $N = 10$.

and 10 are plotted in the top and the bottom panels with the solid line, the dashed line and the circles, corresponding to the variational results obtained with the single D_1 and $D_1^{M=8}$ ansätze and the HEOM results, respectively. The near overlap of the dashed line and the circles further reconfirms the validity of the multi- D_1 ansatz.

Displayed in parts a and c of Figure 7 are the exciton probability $P_{\text{ex}}(t, n)$ and the phonon displacement $X_{\text{ph}}(t, n)$

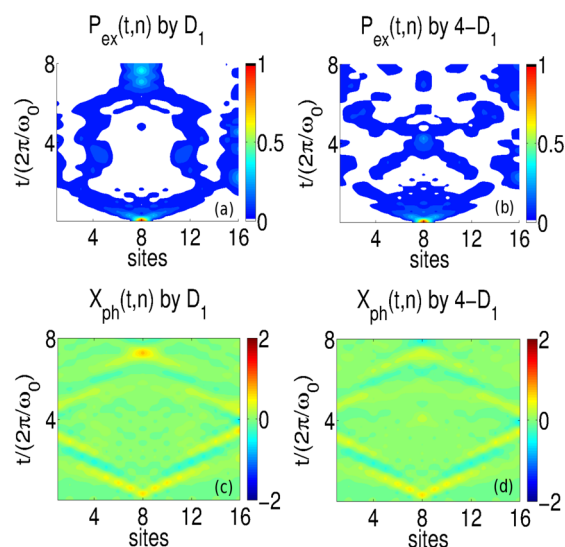


Figure 7. Time evolution of the exciton probability $P_{\text{ex}}(t, n)$ and the phonon displacement $X_{\text{ph}}(t, n)$ obtained with the single D_1 ansatz (left panel) and the $D_1^{M=4}$ ansatz (right panel) are displayed in parts a–d for the case of $W = 0.5$, $g = 0.1$, $J = 0.5$, and $\phi = 0$.

obtained with the single D_1 ansatz, respectively, for the case of $W = 0.5$, $g = 0.1$, $J = 0.5$, and $\phi = 0$. For comparison, corresponding results of $P_{\text{ex}}(t, n)$ and $X_{\text{ph}}(t, n)$ obtained by the multi- D_1 ansatz with $M = 4$ are presented in parts b and d of Figure 7, respectively. Quite obvious difference is found in the excitonic behavior for the two cases when $t/(2\pi/\omega_0) > 3$. Specifically, the exciton probability calculated by the single D_1 ansatz staggers around two sites in the ring before being eventually trapped near site 8 accompanied by a thickened phonon cloud (cf. Figure 7c), while that obtained by the multi- D_1 ansatz with $M = 4$ continues to propagate in two opposite directions. The former behavior is apparently an artifact as the combination of $J = 0.5$ and $g = 0.1$ places the system firmly in the large polaron regime, incompatible with any form of self-trapping at long times. This shows that the single D_1 ansatz is too simplistic to capture accurate polaron dynamics at long times, especially in the weak coupling regime.

Next, we investigate the improvement on the polaron dynamics by the multi- D_2 trial state for the off-diagonal coupling case. The exciton probability $P_{\text{ex}}(t, n)$ calculated by the multi- D_2 ansatz with $M = 16$ for two different sets of the parameters, ($J = 0.1$, $g = 0$, $\phi = 0$, $W = 0.5$) and ($J = 0.1$, $g = 0$, $\phi = 0.1$, $W = 0.5$), are displayed in Figures 8a,b, respectively. Corresponding $P_{\text{ex}}(t, n)$ obtained by the single D_2 ansatz with the same two sets of parameters are shown in Figure 8c,d, which reveals a similar pattern of the exciton motion with the same speed of the exciton packet, $v = \omega_0/2\pi$, despite the increase of the off-diagonal coupling strength from 0 to 0.1. In contrast, the exciton probability obtained with the multi- D_2 ansatz shows localization signatures for off-diagonal coupling strength $\phi = 0.1$, which is absent if $\phi = 0$. It indicates that the combined effect of the transfer integral and the off-diagonal coupling will confine the exciton to the sites of the initial creation, despite that acting alone, either the transfer integral or the off-diagonal coupling may propagate the exciton wave packets. This phenomenon can be better understood after

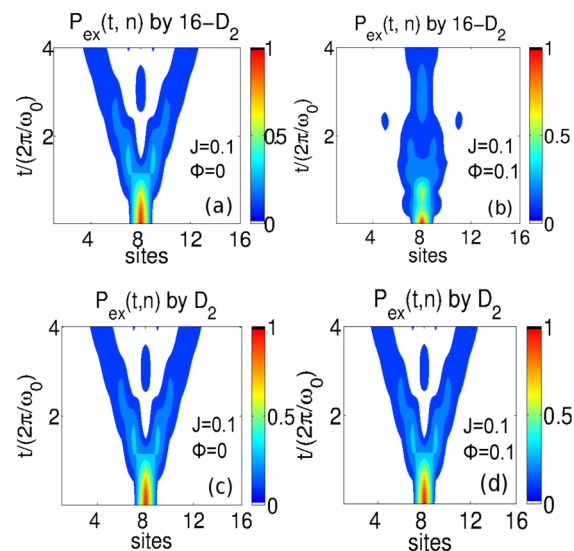


Figure 8. Time evolution of the exciton probability $P_{\text{ex}}(t, n)$ is displayed for the case of $J = 0.1$ and $\phi = 0$ in the left column and the case of $J = 0.1$ and $\phi = 0.1$ in the right column. Other parameters used are $g = 0$, $W = 0.5$, and $N = 16$ for both cases. Two different trial states, the $D_2^{M=16}$ and $D_2^{M=1}$ ansätze, are used in the parts a and b and parts c and d, respectively.

analyzing the energy band near the zone center where a discrete self-trapping transition occurs.³⁶ Our calculations show that effective mass in the case of $\phi = 0.1$ is larger than that of $\phi = 0$, resulting in a less mobile polaron. It demonstrates again that the polaron dynamics obtained with the multiple Davydov trial states is more accurate than that by the single Davydov trial state.

3.3. Absorption Spectra. In this subsection, we employ the multiple Davydov trial states to study the linear absorption spectra $F(\omega)$ defined in eq 19. To facilitate comparisons, spectral maxima are normalized to unity, and a damping factor of $0.08 \omega_0$ is used.^{28,29} In Figure 9, the linear absorption spectra $F(\omega)$ of a 16-site ring is displayed for the case of $g = 0.2$, $J = 0.1$, $W = 0.1$, and $\phi = 0$. In Figure 9a, we compare results obtained by the single D_1 (solid) and single D_2 (dashed) ansätze. Large differences are found between these two curves, and negative values in the spectrum obtained by the single D_2 ansatz point to its apparent invalidity. The multiple D_1 trial states are capable to correct such inaccuracies in its single- D_1 counterpart, as demonstrated in Figure 9b for the multiple D_1 trial state with multiplicity $M = 4$. Similar corrections are also achieved by a multi- D_2 ansatz with a multiplicity of 16, as shown in the same panel. Moreover, the position of the zero-phonon line, denoted by ω_m (in unit of ω_0), is marked by the vertical dash-dotted line at $-0.75(1)$.

The zero-phonon line can be also determined by the ground-state polaron energy band E_k , where k is the crystal momentum. In order to identify the relationship, the transition moment P_k quantifying the transition probability between the vacuum state and the exciton state is introduced and defined as $P_k = \langle 0 | \hat{P} | \Psi_k \rangle$, where $\hat{P} = \mu \sum_n (\hat{a}_n^\dagger |n\rangle_{\text{ex}} \langle n| + |n\rangle_{\text{ex}} \langle n| \hat{a}_n)$ is the polarization operator, and Ψ_k is the ground-state trial wave function with the crystal momentum k . By employing the variational method with the Toyozawa and delocalized D_1 ansätze (details are shown in Appendix C), the ground-state wave function Ψ_k can be obtained, and corresponding polaron energy band $E_k = \langle \Psi_k | \hat{H} | \Psi_k \rangle$ can be calculated accordingly.

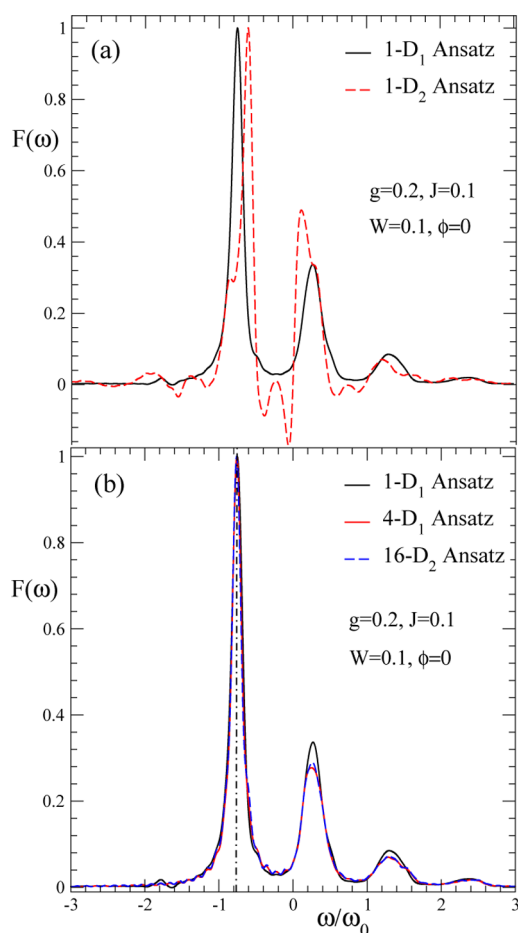


Figure 9. Linear absorption spectra $F(\omega)$ for a 16-site, one-dimensional ring of a coupled exciton–phonon system are displayed in (a) for the single D_1 and D_2 ansätze and in (b) for the single D_1 , $D_1^{M=4}$ and $D_2^{M=16}$ ansätze. The set of parameters $J = 0.1$, $g = 0.2$, $W = 0.1$, and $\phi = 0$ are used. A rescaled factor is adopted to normalize the spectral maxima to facilitate comparisons. The vertical dash-dotted line indicates the location of the zero-phonon line $\omega_m/\omega_0 = -0.75(1)$.

Variational calculations carried out for different k values are independent of each other, and the set of E_k constitutes a variational estimate (an upper bound) for the polaron energy band. In Figure 10, polaron energy bands E_k/ω_0 calculated variationally for the case of $g = 0.2$, $\phi = 0$, $J = 0.1$, and $W = 0.1$, are plotted as a function of the crystal momentum k/π with the solid and open circles corresponding to the delocalized D_1 and the Toyozawa ansätze, respectively. For simplicity, we set $\mu = \omega_0 = 1$. Interestingly, the normalized position of the zero-phonon line, ω_m/ω_0 in Figure 9b, is consistent with the value of $E_{k=0}/\omega_0$. It indicates that $\Psi_{k=0}$ is the bright state responsible for the zero-phonon line, in perfect agreement with the obtained transition probability P_k , which is nonzero only at the crystal momentum $k = 0$ as depicted in the inset.

Moreover, absorption spectra in the presence of off-diagonal coupling ($\phi \neq 0$) are investigated with the aid of a multi- D_2 ansatz with $M = 16$ (we set $J = g = W = 0$ for simplicity). As shown in Figure 11, with an increase in the off-diagonal coupling strength ϕ , phonon sidebands of the linear absorption spectra become broadened and the intensity of the zero-phonon line is reduced. Vertical dashed lines shown in the 4 panels of Figure 11 denote the positions of the zero-phonon lines ($\omega_m/\omega_0 = -0.08, -0.369, -0.956$, and -1.93). For strong

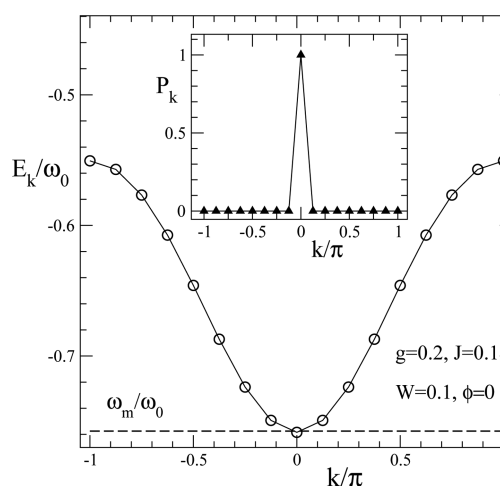


Figure 10. Polaron energy bands E_k/ω_0 are calculated variationally using the delocalized D_1 ansatz (solid line) and the Toyozawa ansatz (open circles) for the case of $g = 0.2$, $J = 0.1$, $W = 0.1$, and $\phi = 0$. The position of the zero-phonon line ω_m/ω_0 is marked by the dashed line, consistent with the values of $E_{k=0}/\omega_0$. A lattice of $N = 16$ sites is used in calculations. In the inset, the transition moment P_k is plotted as a function of the crystal momentum k .

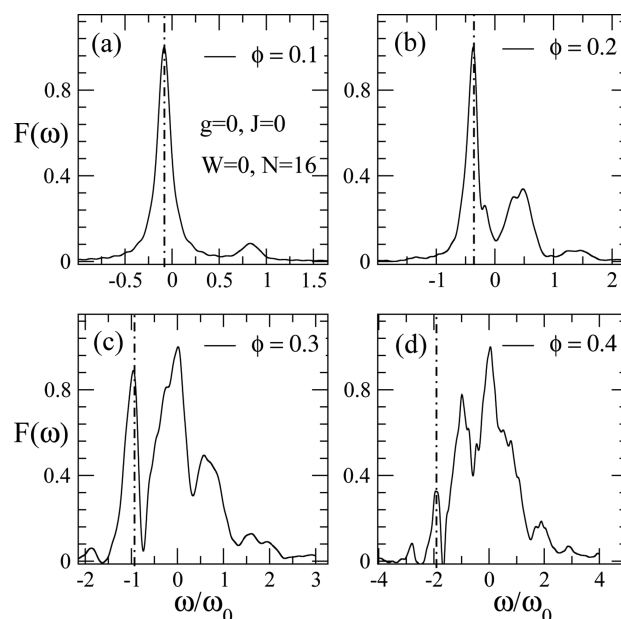


Figure 11. Linear absorption spectra $F(\omega)$ obtained with the $D_2^{M=16}$ ansatz are displayed in parts a–d for the off-diagonal coupling cases with the nonzero coupling strengths $\phi = 0.1, 0.2, 0.3$, and 0.4 , respectively. Other parameters $g = W = J = 0$ and $N = 16$ are set. The vertical dash-dotted lines indicate locations of zero-phonon lines.

off-diagonal coupling, such as the case of $\phi = 1$, the linear absorption spectra, shown in Figure 12, behave quite differently from those in weak off-diagonal coupling cases, such as $\phi = 0.1$ and 0.2 (cf. Figure 11). All of the sharp peaks are smeared out, and the zero-phonon line almost disappears. In order to better understand the line shape, we plot the absorption spectrum in a log–log scale in the inset. A power-law fitting (dashed line) yields a slope of $2.1(1)$ indicating that the phonon sideband deviates from the Gaussian line shape. A Lorentzian line-shape function (dotted line) is then introduced for the fitting,

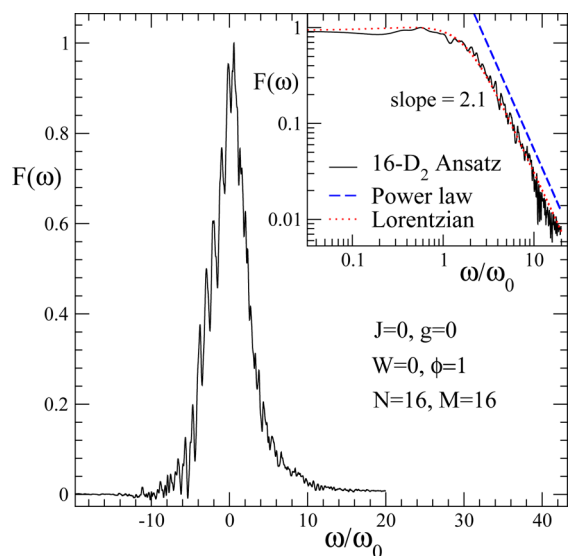


Figure 12. Linear absorption spectrum $F(\omega)$ obtained by the $D_2^{M=16}$ ansatz is displayed for the off-diagonal coupling case with $\phi = 1$. In the inset, the power-law and the Lorentzian fittings are given in the log–log scale with the dashed and dotted lines, respectively.

consistent with the absorption spectrum obtained from the variational method.

3.4. 2D Spectra. In addition to the linear absorption spectra, fast and accurate implementation of the multidimensional spectroscopy is possible via the time-dependent variational method developed here. As an example, we present in this subsection 2D spectra calculated for a molecular ring of 10 sites using the multiple D_2 ansatz. For the secondary bath whose spectral density is defined by eq 53, we adopt the overdamped Brownian oscillator model with the Drude-Lorentz type spectral density

$$D(\omega) = 2\eta \frac{\gamma\omega}{\omega^2 + \gamma^2} \quad (23)$$

The resulting line shape function [cf. eq 58] can be evaluated analytically,⁵⁵

$$g(t) = \frac{\eta}{\gamma} \cot \frac{\gamma\beta}{2} [e^{-\gamma t} + \gamma t - 1] - i \frac{\eta}{\gamma} [e^{-\gamma t} + \gamma t - 1] + \frac{4\eta\gamma}{\beta} \sum_{n=1}^{\infty} \frac{e^{-\nu_n t} + \nu_n t - 1}{\nu_n(\nu_n^2 - \gamma^2)} \quad (24)$$

where $\nu_n = 2\pi n/\beta$ is the Matsubara frequency. In our calculations, we set $\eta = 0.1$, $\beta = 5$, and $\gamma = 0.02$.

In Figure 13, 2D spectra of the 10-site ring are displayed for the case of $\phi = 0.1$ (left panel) and $\phi = 0.4$ (right panel). For simplicity, we set $J = g = W = 0$, and adopt the toy model of J-aggregates with the tangential (head-to-tail) orientations of the transition dipoles. We first consider weak off-diagonal coupling ($\phi = 0.1$). The 2D spectra are shown in parts a–c of Figure 13, corresponding to the population times $T = 0, 20$, and 40, respectively. At $T = 0$, the signal exhibits a single peak located at $(\omega_r, \omega_i) = (-0.08, -0.08)$, which is elongated along the diagonal line. As the population time increases, the elongation becomes less pronounced, and the peak appears more rounded. We then study the case of strong off-diagonal coupling with $\phi = 0.4$, as depicted in the right column of Figure 13 for several

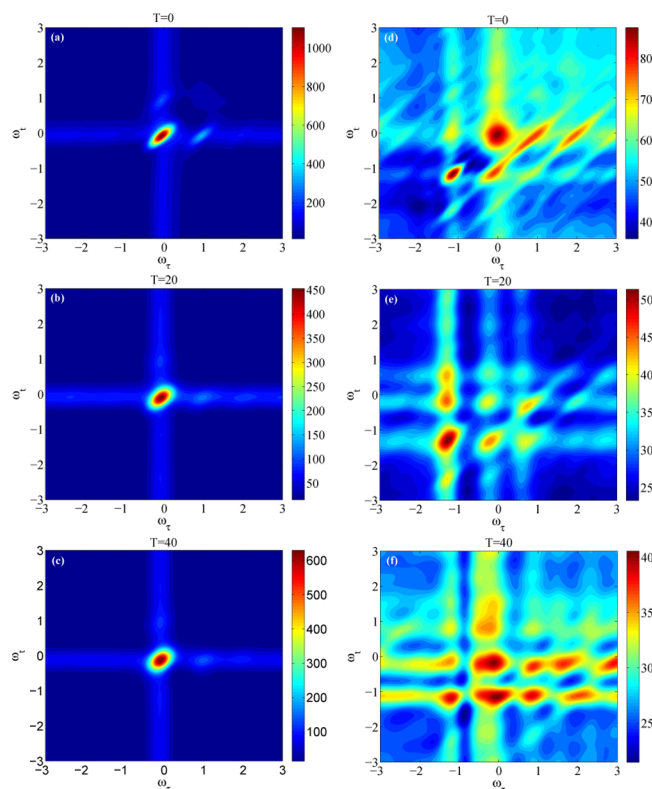


Figure 13. 2D spectra of the molecular ring for off-diagonal coupling strengths $\phi = 0.1$ (left column) and $\phi = 0.4$ (right column). Upper, middle and lower panels correspond to the population time $T = 0, 20$, and 40, respectively. Other parameters $g = W = J = 0$ and $N = 10$ are set.

values of the population time (see Figure 13, parts d–f for $T = 0, 20$, and 40, respectively). Overall, it is found that strong exciton phonon coupling induces a pronounced vibronic multipeak structure in the 2D spectra. With increasing population time, the shapes as well as the strengths for the peaks change, and we also find population cascades from high to low energy regions with lower ω_i for larger values of T , as demonstrated in Figure 13d–f.

4. CONCLUSIONS

In this work, we have studied the dynamical properties of the Holstein polaron in a one-dimensional molecular ring using the Dirac–Frenkel time-dependent variational principle and an extended form of the Davydov trial states, also known as the “multi- D_1 ansatz” (“multi- D_2 ansatz”), which is a linear combination of the single Davydov D_1 (D_2) trial states. For both diagonal and off-diagonal exciton–phonon coupling, the relative error quantifying how closely the trial state follows the Schrödinger equation is found to decrease with the multiplicity M , reflecting the improvement in accuracy of the multiple Davydov trial states. Moreover, exciton probabilities calculated by the multiple Davydov trial states are obtained, in perfect agreement with those from a numerically exact approach employing the hierarchy equations of motion, demonstrating the great promise the multiple Davydov trial states hold as an efficient, robust description of dynamics of the complex quantum systems.

An abnormal self-trapping phenomenon is uncovered in the dynamical behavior of polaron with the increase of the off-diagonal coupling. Besides, the optical spectrum is also studied

as a sensitive indicator of the accuracy of the variational polaron dynamics. Among our findings, linear absorption spectra from the multi-D₁ *ansatz* with a multiplicity of 4 can be reproduced by the multi-D₂ *ansatz* with a multiplicity of 16, and the positions of the zero-phonon lines are in good agreement with ground-state energy bands calculated by the Toyozawa and the delocalized D₁ *ansätze* in the weak electronic coupling (transfer integral) regime. Moreover, for the first time, 2D spectra have been calculated for systems with off-diagonal exciton–phonon coupling by employing the multiple D₂ *ansatz* to compute the nonlinear response function, testifying to the great potential of the multiple D₂ *ansatz* for fast, accurate implementation of multidimensional spectroscopy. It is also found that the signal exhibits a single peak for weak off-diagonal coupling, while a vibronic multipeak structure appears for strong off-diagonal coupling.

APPENDIX A. THE MULTI-D₁ TRIAL STATE

The individual energy terms can be respectively calculated as follows:

$$\langle D_1^M(t) | H_{\text{ex}} | D_1^M(t) \rangle = -J \sum_{i,j} \sum_n \psi_{j,n}^*(t) [\psi_{i,n+1}(t) S_{j,n;i,n+1} + \psi_{i,n-1}(t) S_{j,n;i,n-1}] \quad (25)$$

$$\langle D_1^M(t) | H_{\text{ph}} | D_1^M(t) \rangle = \sum_{i,j} \sum_n \psi_{j,n}^* \psi_{i,n} \sum_q \omega_q \lambda_{jnq}^* \lambda_{inq} S_{ji} \quad (26)$$

$$\langle D_1^M(t) | H_{\text{ex-ph}}^{\text{diag}} | D_1^M(t) \rangle = -g \sum_{i,j} \sum_n \psi_{j,n}^* \psi_{i,n} \times \sum_q \omega_q (e^{iqn} \lambda_{inq} + e^{-iqn} \lambda_{jnq}^*) S_{ji} \quad (27)$$

$$\langle D_1^M(t) | H_{\text{ex-ph}}^{\text{o.d.}} | D_1^M(t) \rangle = \frac{1}{2} \phi \sum_{n,q} \sum_{i,j} \omega_q S_{j,n;i,n+1} \psi_{j,n}^*(t) \times \psi_{i,n+1}(t) [e^{iqn} (e^{iq} - 1) \lambda_{i,n+1,q}(t) + e^{-iqn} (e^{-iq} - 1) \times \lambda_{jnq}^*(t)] + \frac{1}{2} \phi \sum_{n,q} \sum_{i,j} \omega_q S_{j,n;i,n-1} \psi_{j,n}^*(t) \psi_{i,n-1}(t) [e^{iqn} (1 - e^{-iq}) \lambda_{i,n-1,q}(t) + e^{-iqn} (1 - e^{iq}) \lambda_{jnq}^*(t)] \quad (28)$$

where the Debye–Waller factor is formulated as

$$S_{ij} = \langle \lambda_i | \lambda_j \rangle, \quad S_{j,n;i,n+1} = \langle \lambda_{j,n} | \lambda_{i,n+1} \rangle \quad (29)$$

The Dirac–Frenkel variational principle leads to equations of motion:

$$-i \sum_i \dot{\psi}_{in} S_{ki} - \frac{i}{2} \sum_i \psi_{in} \sum_q (2\lambda_{knq}^* \lambda_{inq} - \lambda_{inq} \lambda_{in}^* - \lambda_{in} \lambda_{knq}^*) \times S_{k,i} = J \sum_i (\psi_{i,n+1} S_{k,n;i,n+1} + \psi_{i,n-1} S_{k,n;i,n-1}) - \sum_i \psi_{in} \sum_q \omega_q \lambda_{knq}^* \lambda_{inq} S_{ki} + g \sum_i \psi_{in} \sum_q \omega_q \times (e^{iqn} \lambda_{inq} + e^{-iqn} \lambda_{knq}^*) S_{ki} - \frac{1}{2} \phi \sum_i \sum_q \omega_q \psi_{i,n+1}(t) \times [e^{iqn} (e^{iq} - 1) \lambda_{i,n+1,q}(t) + e^{-iqn} (e^{-iq} - 1) \lambda_{knq}^*(t)] \times S_{k,n;i,n+1} - \frac{1}{2} \phi \sum_i \sum_q \omega_q \psi_{i,n-1}(t) [e^{iqn} (1 - e^{-iq}) \times \lambda_{i,n-1,q}(t) + e^{-iqn} (1 - e^{iq}) \lambda_{knq}^*(t)] S_{k,n;i,n-1} \quad (30)$$

$$-i \sum_i \psi_{kn}^* \dot{\psi}_{in} \lambda_{inq} S_{ki} - i \sum_i \psi_{kn}^* \psi_{in} \dot{\lambda}_{inq} S_{ki} - \frac{i}{2} \sum_i \psi_{kn}^* \psi_{in} \lambda_{inq} \times S_{k,i} \sum_p (2\lambda_{knp}^* \lambda_{inp} - \lambda_{inp} \lambda_{kn}^* - \lambda_{kn} \lambda_{inp}^*) = J \sum_i \psi_{k,n}^* (\psi_{i,n+1} \lambda_{i,n+1,q} S_{k,n;i,n+1} + \psi_{i,n-1} \lambda_{i,n-1,q} \times S_{k,n;i,n-1}) - \sum_i \psi_{kn}^* \psi_{in} \lambda_{inq} S_{ki} (\omega_q + \sum_p \omega_p \lambda_{knp}^* \lambda_{inp}) + g \sum_i \psi_{kn}^* \psi_{in} \omega_q e^{-iqn} S_{ki} + g \sum_i \psi_{kn}^* \psi_{in} \lambda_{inq} \sum_p \omega_p \times (e^{ipn} \lambda_{inp} + e^{-ipn} \lambda_{knp}^*) S_{k,i} - \frac{1}{2} \phi \sum_i \omega_q \psi_{kn}^* [\psi_{i,n+1} e^{-iqn} \times (e^{-iq} - 1) S_{k,n;i,n+1} + \psi_{i,n-1} e^{-iqn} (1 - e^{iq}) S_{k,n;i,n-1}] - \frac{1}{2} \phi \sum_p \sum_i \omega_p \psi_{k,n}^* \psi_{i,n+1} [e^{ipn} (e^{ip} - 1) \lambda_{i,n+1,p} + e^{-ipn} (e^{-ip} - 1) \lambda_{knp}^*] \lambda_{i,n+1,q} S_{k,n;i,n+1} - \frac{1}{2} \phi \sum_p \sum_i \omega_p \psi_{k,n}^* \psi_{i,n-1} [e^{ipn} (1 - e^{-ip}) \lambda_{i,n-1,p} + e^{-ipn} (1 - e^{ip}) \lambda_{knp}^*] \lambda_{i,n-1,q} S_{k,n;i,n-1} \quad (31)$$

APPENDIX B. HIERARCHY EQUATION OF MOTION

For the Holstein model [eq 1], let us denote $|n\rangle = \hat{a}_n^\dagger |0\rangle_{\text{ex}}$ where $|0\rangle_{\text{ex}}$ stands for the exciton vacuum. Then the reduced density matrix element for the exciton system is expressed in the path integral form with the factorized initial condition as⁶²

$$\rho(n, n'; t) = \int \mathcal{D}n \int \mathcal{D}n' \rho(n_0, n'_0; t_0) \times e^{iS[n;t]} F(n, n'; t) e^{-iS[n';t]} \quad (32)$$

where $S[n]$ is an action of the exciton system and $F[n, n']$ is the Feynman–Vernon influence functional

$$F[n, n'] = \exp\left(-\sum_q \omega_q^2 \int_{t_0}^t ds \int_{t_0}^s ds' V_q^{*\times}(s)\right. \\ \left. \times [V_q^\times(s') \coth(\beta\omega_q/2) \cos(\omega_q(s-s'))\right. \\ \left. - iV_q^\circ(s') \sin(\omega_q(s-s'))]\right). \quad (33)$$

In the above equation, β is the inverse of temperature ($\beta = 1/k_B T$), and the abbreviations

$$V_q^\times = V_q(n) - V_q(n'), \quad V_q^\circ = V_q(n) + V_q(n') \quad (34)$$

are introduced with $\hat{V}_q^\dagger = g \sum_n \hat{a}_n^\dagger \hat{a}_n e^{iqn}$.

eq 33 can be rewritten as

$$F[n, n'] = \exp\left(-\sum_q \omega_q^2 \int_{t_0}^t ds \int_{t_0}^s ds' V_q^{*\times}(s)\right. \\ \left. \times \left[\frac{e^{i\omega_q(s-s')}}{2} (V_q^\times(s') \coth(\beta\omega_q/2) - V_q^\circ(s'))\right.\right. \\ \left. \left. + \frac{e^{-i\omega_q(s-s')}}{2} (V_q^\times(s') \coth(\beta\omega_q/2) + V_q^\circ(s'))\right]\right) \quad (35)$$

Taking derivative of eq 32, one has

$$\frac{\partial}{\partial t} \rho(n, n'; t) = -i\mathcal{L}\rho(n, n'; t) \\ - \sum_q \omega_q^2 V_q^{*\times}(t) \int \mathcal{D}n \int \mathcal{D}n' \rho(n_0, n'_0; t_0) \\ \times \int_0^t ds' \left[\frac{e^{i\omega_q(t-s')}}{2} (V_q^\times(s') \coth(\beta\omega_q/2) - V_q^\circ(s'))\right. \\ \left. + \frac{e^{-i\omega_q(t-s')}}{2} (V_q^\times(s') \coth(\beta\omega_q/2) + V_q^\circ(s')) \right] \\ \times e^{iS[n,t]} F(n, n'; t) e^{-iS[n',t]} \quad (36)$$

If we use the following superoperator

$$\hat{\Phi}_q(t) = \omega_q^2 V_q^{*\times}(t)/2, \\ \hat{\Theta}_{q\pm}(t) = V_q^\times(t) \coth(\beta\omega_q/2) \mp V_q^\circ(t) \quad (37)$$

Equations 35 and 36 then can be simplified as

$$F[n, n'] = \exp\left(-\sum_q \int_{t_0}^t ds \int_{t_0}^s ds' \Phi_q(s)\right. \\ \left. \times [e^{i\omega_q(s-s')} \Theta_{q+}(s') + e^{-i\omega_q(s-s')} \Theta_{q-}(s')]\right) \quad (38)$$

$$\frac{\partial}{\partial t} \rho(n, n'; t) = -i\mathcal{L}\rho(n, n'; t) \\ - \sum_q \Phi_q(t) \int \mathcal{D}n \int \mathcal{D}n' \rho(n_0, n'_0; t_0) \\ \times \int_0^t ds' [e^{i\omega_q(t-s')} \Theta_{q+}(s') \\ + e^{-i\omega_q(t-s')} \Theta_{q-}(s')] \times e^{iS[n,t]} F(n, n'; t) e^{-iS[n',t]} \quad (39)$$

In order to derive the equations of motion, we introduce the auxiliary operator $\rho_{m_{1\pm}, m_{2\pm}, \dots, m_{N\pm}}(n, n'; t)$ by its matrix element as

$$\rho_{m_{1\pm}, m_{2\pm}, \dots, m_{N\pm}}(n, n'; t) \\ = \int \mathcal{D}n \int \mathcal{D}n' \rho(n_0, n'_0; t_0) \prod_{q=1}^N \left(\int_{t_0}^t ds e^{i\omega_q(t-s)} \Theta_{q+}(s) \right)^{m_{q+}} \\ \times \left(\int_{t_0}^t ds e^{-i\omega_q(t-s)} \Theta_{q-}(s) \right)^{m_{q-}} \times e^{iS[n,t]} F(n, n') e^{-iS[n',t]} \quad (40)$$

for non-negative integers $m_{1\pm}, m_{2\pm}, \dots, m_{N\pm}$. Note that only $\hat{\rho}_{0\dots 0}(t) = \hat{\rho}(t)$ has a physical meaning and the others are introduced for computational purposes only. Differentiating $\rho_{m_{1\pm}, m_{2\pm}, \dots, m_{N\pm}}(n, n'; t)$ with respect to t , we can obtain the following hierarchy of equations in the operator form:

$$\frac{\partial}{\partial t} \hat{\rho}_{m_{1\pm}, \dots, m_{N\pm}}(t) = -i\mathcal{L} \hat{\rho}_{m_{1\pm}, \dots, m_{N\pm}}(t) \\ - i \sum_q \omega_q (m_{q-} - m_{q+}) \hat{\rho}_{m_{1\pm}, \dots, m_{N\pm}}(t) \\ - \sum_q \hat{\Phi}_q (\hat{\rho}_{m_{1\pm}, \dots, m_{q+}+1, m_{q-}, \dots, m_{N\pm}}(t) \\ + \hat{\rho}_{m_{1\pm}, \dots, m_{q+}, m_{q-}+1, \dots, m_{N\pm}}(t)) \\ + \sum_q (m_{q+} \hat{\Theta}_{q+} \hat{\rho}_{m_{1\pm}, \dots, m_{q+}-1, m_{q-}, \dots, m_{N\pm}}(t) \\ + m_{q-} \hat{\Theta}_{q-} \hat{\rho}_{m_{1\pm}, \dots, m_{q+}, m_{q-}-1, \dots, m_{N\pm}}(t)) \quad (41)$$

The HEOM consists of an infinite number of equations, but they can be truncated using a number of hierarchy elements. The infinite hierarchy of eq 41 can be truncated by the terminator as

$$\frac{\partial}{\partial t} \hat{\rho}_{m_{1\pm}, \dots, m_{N\pm}}(t) = -(i\mathcal{L} + i \sum_q \omega_q (m_{q-} - m_{q+})) \\ \times \hat{\rho}_{m_{1\pm}, \dots, m_{N\pm}}(t) \quad (42)$$

The total number of hierarchy elements can be evaluated as $L_{\text{tot}} = (N_{\text{trun}} + 2N)!/N_{\text{trun}}!(2N)!$, while the total number of termination elements is $L_{\text{term}} = (N_{\text{trun}} + 2N - 1)!/(2N - 1)! N_{\text{trun}}!$, where N_{trun} is the depth of the hierarchy for $m_{q\pm}$ ($q = 1, \dots, N$). In practice, we can set the termination elements to zero and thus the number of hierarchy elements for the calculation can be reduced as $L_{\text{calc}} = L_{\text{tot}} - L_{\text{term}}$.

■ APPENDIX C. DELOCALIZED D_1 ANSATZ AND THE TOYOZAWA ANSATZ

Our interest in this work includes the polaron ground-state energy band, computed as

$$E(\kappa) = \langle \Psi(\kappa) | \hat{H} | \Psi(\kappa) \rangle \quad (43)$$

where $|\Psi(\kappa)\rangle$ is an appropriately normalized, delocalized trial state, and \hat{H} is the system Hamiltonian. The joint crystal momentum is indicated by the Greek κ . It should be noted that the crystal momentum operator commutes with the system Hamiltonian, and energy eigenstates are also eigenfunctions of the crystal momentum. Therefore, variations for distinct κ are independent. The set of $E(\kappa)$ constitutes a variational estimate

(an upper bound) for the polaron energy band. The relaxation iteration technique, viewed as an efficient method for identifying energy minima of a complex variational system, is adopted in this work to obtain numerical solutions to a set of self-consistency equations derived from the variational principle. To achieve efficient and stable iterations toward the variational ground state, one may take advantage of the continuity of the ground state with respect to small changes in system parameters over most of the phase diagram and may initialize the iteration using a reliable ground state already determined at some nearby points in parameter space. Starting from those limits where exact solutions can be obtained analytically and executing a sequence of variations along well-chosen paths through the parameter space using solutions from one step to initialize the next, the whole parameter space can be explored.

The D_1 and D_2 *ansätze* are localized states from the soliton theory, but without considering a form factor of a delocalized state. The polaron state have been analyzed with the delocalized D_1 and Toyozawa *ansätze*, both of which are Bloch states with the designated crystal momentum. The D_1 and D_2 *ansätze* can be transformed to the delocalized D_1 and Toyozawa *ansätze* via a projection operator \hat{P}_κ

$$\hat{P}_\kappa = N^{-1} \sum_n e^{i(\kappa - \hat{p})n} = \delta(\kappa - \hat{p}) \quad (44)$$

where

$$\hat{P} = \sum_k ka_k^\dagger a_k + \sum_q qb_q^\dagger b_q \quad (45)$$

The delocalized D_1 *ansatz* are then obtained after the delocalization onto the usual D_1 *ansatz*

$$|\Psi_1(\kappa)\rangle = |\kappa\rangle \langle \kappa | \kappa \rangle^{-1/2} \quad (46)$$

$$|\kappa\rangle = \sum_n e^{i\kappa n} \sum_{n_1} \alpha_{n_1-n}^\kappa a_{n_1}^\dagger \times \exp[-\sum_{n_2} (\beta_{n_1-n, n_2-n}^\kappa b_{n_2}^\dagger - \text{H. c.})] |0\rangle \quad (47)$$

where H.c. stands for the Hermitian conjugate, $|0\rangle$ is the product of the exciton and phonon vacuum states, $\alpha_{n_1-n}^\kappa$ is the exciton amplitude, and the phonon displacement $\beta_{n_1-n, n_2-n}^\kappa$ depends on n_1 and n_2 , respectively, the sites at which an electronic excitation and a phonon are generated.

After the delocalization onto the usual D_2 *ansatz*, the Toyozawa *ansatz* is given by

$$|\Psi_2(\kappa')\rangle = |\kappa'\rangle \langle \kappa' | \kappa' \rangle^{-1/2} \quad (48)$$

$$|\kappa'\rangle = \sum_n e^{i\kappa' n} \sum_{n_1} \psi_{n_1-n}^{\kappa'} a_{n_1}^\dagger \times \exp[-\sum_{n_2} (\lambda_{n_2-n}^{\kappa'} b_{n_2}^\dagger - \text{H. c.})] |0\rangle \quad (49)$$

where $\psi_{n_1-n}^{\kappa'}$ is the exciton amplitude analogous to $\alpha_{n_1-n}^\kappa$ in the delocalized D_1 *ansatz*, and $\lambda_{n_2-n}^{\kappa'}$ is the phonon displacement. Actually, $\lambda_{n_2-n}^{\kappa'}$ is just one column of the phonon displacement matrix $\beta_{n_1-n, n_2-n}^\kappa$ in the delocalized D_1 *ansatz*.

■ APPENDIX D. SIMULATION OF 2D SPECTRA USING MULTIPLE D_2 ANSÄTZE

In order to describe the population decays and dephasings induced by solvent, we add additional term $H_B + H_{SB}$ to the Hamiltonian 1

$$\begin{aligned} \hat{H} &= \hat{H}_{ex} + \hat{H}_{ph} + \hat{H}_{ex-ph}^{diag} + \hat{H}_{ex-ph}^{o.d.} + \hat{H}_B + \hat{H}_{SB} \\ &= \hat{H}_S + \hat{H}_B + \hat{H}_{SB} \end{aligned} \quad (50)$$

where we have included vibrational modes with significant exciton–phonon coupling into system Hamiltonian, i.e., $\hat{H}_S = \hat{H}_{ex} + \hat{H}_{ph} + \hat{H}_{ex-ph}^{diag} + \hat{H}_{ex-ph}^{o.d.}$ and treated the rest of vibrational modes as a heat bath. We assume a harmonic bath with site-independent and diagonal system bath coupling^{56,57,63}

$$\hat{H}_B = \sum_j \hbar \Omega_j c_j^\dagger c_j \quad (51)$$

$$\hat{H}_{SB} = \sum_j \sum_{n=1}^N \kappa_j \hbar \Omega_j (c_j^\dagger + c_j) a_n^\dagger a_n \quad (52)$$

Here, c_j (c_j^\dagger) is the annihilation (creation) operator of the j th bath mode with frequency Ω_j and κ_j is the corresponding exciton-bath coupling strength. The bath spectral density is specified by

$$D(\omega) = \sum_j \kappa_j^2 \Omega_j^2 \delta(\omega - \Omega_j) \quad (53)$$

It is noted that system-bath Hamiltonian \hat{H}_{SB} commutes with the system Hamiltonian \hat{H}_S , and as a result, the nonlinear response function can be represented as a product of the system and bath. Furthermore, by making use of the fact that the system-bath coupling is the same for all excitons, the effect of bath can be taken into account through line shape factors F_i in the framework of second-order cumulant expansion. Finally, we arrived at the formulas for the nonlinear response function⁵⁶

$$\begin{aligned} R_1(t, T, \tau) &= F_1(t, T, \tau) \sum_{n, n', n'', n'''} C_{n, n', n'', n'''} \\ &\times_{\text{ph}} \langle 0 | \langle n | e^{iH_S T} | n' \rangle \langle n'' | e^{-H_S(t+T+\tau)} | n''' \rangle | 0 \rangle_{\text{ph}} \\ R_2(t, T, \tau) &= F_2(t, T, \tau) \sum_{n, n', n'', n'''} C_{n, n', n'', n'''} \\ &\times_{\text{ph}} \langle 0 | \langle n | e^{iH_S(\tau+T)} | n' \rangle \langle n'' | e^{-H_S(t+T)} | n''' \rangle | 0 \rangle_{\text{ph}} \\ R_3(t, T, \tau) &= F_3(t, T, \tau) \sum_{n, n', n'', n'''} C_{n, n', n'', n'''} \\ &\times_{\text{ph}} \langle 0 | \langle n | e^{iH_S \tau} | n' \rangle \langle n'' | e^{-H_S t} | n''' \rangle | 0 \rangle_{\text{ph}} \\ R_4(t, T, \tau) &= F_4(t, T, \tau) \sum_{n, n', n'', n'''} C_{n, n', n'', n'''} \\ &\times_{\text{ph}} \langle 0 | \langle n | e^{-iH_S t} | n' \rangle \langle n'' | e^{-H_S \tau} | n''' \rangle | 0 \rangle_{\text{ph}} \end{aligned} \quad (54)$$

Here

$$C_{n, n', n'', n'''} = (\mathbf{e}_1 \mu_n) (\mathbf{e}_2 \mu_{n'}) (\mathbf{e}_3 \mu_{n''}) (\mathbf{e}_4 \mu_{n'''}) \quad (55)$$

are the geometrical factors which must be averaged over orientations of the transition dipole moments μ_n . For simplicity, we can assume all laser fields have the same polarization, then the averaging can be done analytically, leading to

$$C_{n,n',n'',n'''} = \frac{1}{15} ((\mu_n \mu_{n'}) (\mu_{n''} \mu_{n'''})) + (\mu_n \mu_{n''}) (\mu_{n'} \mu_{n'''}) + (\mu_n \mu_{n'''}) (\mu_{n'} \mu_{n''}) \quad (56)$$

The line shape factors F_i can be easily evaluated as⁵⁵

$$\begin{aligned} F_1(t, T, \tau) &= e^{-g^*(t)-g(\tau)-g^*(T)+g^*(T+t)+g(\tau+T)-g(\tau+T+t)} \\ F_2(t, T, \tau) &= e^{-g^*(t)-g^*(\tau)+g(T)-g(T+t)-g^*(\tau+T)+g^*(\tau+T+t)} \\ F_3(t, T, \tau) &= e^{-g(t)-g^*(\tau)+g^*(T)-g^*(T+t)-g^*(\tau+T)+g^*(\tau+T+t)} \\ F_4(t, T, \tau) &= e^{-g(t)-g(\tau)-g(T)+g(T+t)+g(\tau+T)-g(\tau+T+t)} \end{aligned} \quad (57)$$

where $g(t)$ is the line shape function

$$g(t) = \int_0^\infty d\omega \frac{D(\omega)}{\omega^2} \times \left[\coth \frac{\hbar\omega\beta}{2} (1 - \cos \omega t) + i(\sin \omega t - \omega t) \right] \quad (58)$$

The next crucial step is to approximate the propagator in terms of the multiple D_2 ansatz, i.e.,

$$e^{-iH_t|n\rangle\langle 0|}_{ph} = \sum_i^M \sum_n^N \psi_{i,n} \hat{a}_n^\dagger |0\rangle_{ex} \exp\left\{ \sum_q [\lambda_{iq} \hat{b}_q^\dagger - \lambda_{iq}^* \hat{b}_q] \right\} |0\rangle_{ph} \quad (59)$$

Explicitly, we have final expressions for the nonlinear response function

$$\begin{aligned} R_1(t, T, \tau) &= F_1(t, T, \tau) \sum_{n,n',n'',n'''} C_{n,n',n'',n'''} \sum_{i,j=1}^M \psi_{jn}^{n''*}(T) \\ &\quad \times \psi_{in}^{n''}(\tau + T + t) e^{-1/2 \sum_q (\lambda_{jq}^n(T)^2 + \lambda_{iq}^{n''}(\tau+T+t)^2)} \\ &\quad \times e^{\sum_q \lambda_{jq}^{n''}(T) \lambda_{iq}^{n''}(\tau+T+t) e^{i\omega_q t}} \\ R_2(t, T, \tau) &= F_2(t, T, \tau) \sum_{n,n',n'',n'''} C_{n,n',n'',n'''} \sum_{i,j=1}^M \psi_{jn}^{n''*}(T + \tau) \\ &\quad \times \psi_{in}^{n''}(T + t) e^{-1/2 \sum_q (\lambda_{jq}^n(T+\tau)^2 + \lambda_{iq}^{n''}(T+t)^2)} \\ &\quad \times e^{\sum_q \lambda_{jq}^{n''}(T+\tau) \lambda_{iq}^{n''}(T+t) e^{i\omega_q t}} \\ R_3(t, T, \tau) &= F_3(t, T, \tau) \sum_{n,n',n'',n'''} C_{n,n',n'',n'''} \sum_{i,j=1}^M \psi_{jn}^{n''*}(\tau) \\ &\quad \times \psi_{in}^{n''}(t) e^{-1/2 \sum_q (\lambda_{jq}^n(\tau)^2 + \lambda_{iq}^{n''}(t)^2)} \\ &\quad \times e^{\sum_q \lambda_{jq}^{n''}(\tau) \lambda_{iq}^{n''}(t) e^{i\omega_q(\tau+t)}} \\ R_4(t, T, \tau) &= F_4(t, T, \tau) \sum_{n,n',n'',n'''} C_{n,n',n'',n'''} \sum_{i,j=1}^M \psi_{jn}^{n''*}(-t) \\ &\quad \times \psi_{in}^{n''}(\tau) e^{-1/2 \sum_q (\lambda_{jq}^n(-t)^2 + \lambda_{iq}^{n''}(\tau)^2)} \\ &\quad \times e^{\sum_q \lambda_{jq}^{n''}(-t) \lambda_{iq}^{n''}(\tau) e^{-i\omega_q \tau}} \end{aligned} \quad (60)$$

AUTHOR INFORMATION

Corresponding Author

* (Y.Z.) E-mail: yzhao@ntu.edu.sg. Telephone: +(65) 65137990.

Notes

The authors declare no competing financial interest.

ACKNOWLEDGMENTS

The authors thank Vladimir Chernyak for insightful discussion and Jiangfeng Zhu for help with numerics. Support from the Singapore National Research Foundation through the Competitive Research Programme (CRP) under Project No. NRF-CRP5-2009-04 is gratefully acknowledged. N.Z. and K.S. are also supported in part by the National Natural Science Foundation of China under Grant Nos. 11205043, 11404084, and 11574052.

REFERENCES

- (1) An, Z.; Wu, C. Q.; Sun, X. Dynamics of Photogenerated Polarons in Conjugated Polymers. *Phys. Rev. Lett.* **2004**, *93* (21), 216407.
- (2) Zheng, B.; Wu, J.; Sun, W.; Liu, C. Trapping and Hopping of Polaron in DNA Periodic Stack. *Chem. Phys. Lett.* **2006**, *425* (1–3), 123–127.
- (3) Liu, X.; Gao, K.; Fu, J.; Li, Y.; Wei, J.; Xie, S. Effect of the Electric Field Mode on the Dynamic Process of a Polaron. *Phys. Rev. B: Condens. Matter Mater. Phys.* **2006**, *74* (17), 172301.
- (4) Bronner, C.; Tegeder, P. Relaxation Dynamics of Photoexcited Charge Carriers at the Bi(111) Surface. *Phys. Rev. B: Condens. Matter Mater. Phys.* **2014**, *89* (11), 115105.
- (5) Timrov, I.; Kampfrath, T.; Faure, J.; Vast, N.; Ast, C. R.; Frischkorn, C.; Wolf, M.; Gava, P.; Perfetti, L. Thermalization of Photoexcited Carriers in Bismuth Investigated by Time-Resolved Terahertz Spectroscopy and Ab Initio Calculations. *Phys. Rev. B: Condens. Matter Mater. Phys.* **2012**, *85* (15), 155139.
- (6) Chikan, V.; Kelley, D. F. Relaxation Dynamics in Photoexcited GaSe Nanoparticles. *J. Chem. Phys.* **2002**, *117* (19), 8944–8952.
- (7) Klimov, V. I.; Mikhailovsky, A. A.; McBranch, D. W.; Leatherdale, C. A.; Bawendi, M. G. Mechanisms for Intraband Energy Relaxation in Semiconductor Quantum Dots: The Role of Electron-Hole Interactions. *Phys. Rev. B: Condens. Matter Mater. Phys.* **2000**, *61* (20), R13349–R13352.
- (8) Kim, S. H.; Wolters, R. H.; Heath, J. R. Photophysics of Size-Selected InP Nanocrystals: Exciton Recombination Kinetics. *J. Chem. Phys.* **1996**, *105* (18), 7957–7963.
- (9) Sauer, K. Photosynthesis-The Light Reactions. *Annu. Rev. Phys. Chem.* **1979**, *30* (1), 155–178.
- (10) Renger, T.; May, V.; Kühn, O. Ultrafast Excitation Energy Transfer Dynamics in Photosynthetic Pigment–protein Complexes. *Phys. Rep.* **2001**, *343* (3), 137–254.
- (11) Blankenship, R. E. *Molecular Mechanisms of Photosynthesis*; Blackwell Science: Oxford and Malden, U.K., 2002.
- (12) Van Grondelle, R.; Novoderezhkin, V. I. Energy Transfer in Photosynthesis: Experimental Insights and Quantitative Models. *Phys. Chem. Chem. Phys.* **2006**, *8* (7), 793–807.
- (13) Chen, L.; Shenai, P.; Zheng, F.; Somoza, A.; Zhao, Y. Optimal Energy Transfer in Light-Harvesting Systems. *Molecules* **2015**, *20* (8), 15224–15272.
- (14) Tomimoto, S.; Nansei, H.; Saito, S.; Suemoto, T.; Takeda, J.; Kurita, S. Femtosecond Dynamics of the Exciton Self-Trapping Process in a Quasi-One-Dimensional Halogen-Bridged Platinum Complex. *Phys. Rev. Lett.* **1998**, *81* (2), 417–420.
- (15) Dexheimer, S.; Van Pelt, A. D.; Brozik, J.; Swanson, B. Femtosecond Vibrational Dynamics of Self-Trapping in a Quasi-One-Dimensional System. *Phys. Rev. Lett.* **2000**, *84* (19), 4425–4428.
- (16) Sugita, A.; Saito, T.; Kano, H.; Yamashita, M.; Kobayashi, T. Wave Packet Dynamics in a Quasi-One-Dimensional Metal-Halogen

Complex Studied by Ultrafast Time-Resolved Spectroscopy. *Phys. Rev. Lett.* **2001**, *86* (10), 2158–2161.

(17) Morrissey, F. X.; Dexheimer, S. L. Coherent Acoustic Phonon Generation in Exciton Self-Trapping. *Phys. Rev. B: Condens. Matter Mater. Phys.* **2010**, *81* (9), 094302.

(18) Alexandrov, A. S.; Mott, N. *Polarons and Bipolarons*; World Scientific: London, 1995.

(19) Osaka, Y. Theory of Polaron Mobility. *Prog. Theor. Phys.* **1961**, *25* (4), 517–536.

(20) Ranninger, J. In *Polarons in Bulk Materials and Systems with Reduced Dimensionality*; Iadonisi, G., Ranninger, J., De Filippis, G., Eds.; International School of Physics Enrico Fermi; IOS Press: Amsterdam, 2006; Vol. 161, p 1.

(21) Holstein, T. Studies of Polaron Motion Part 1. The Molecular-Crystal Model. *Ann. Phys. (Amsterdam, Neth.)* **1959**, *8*, 325–342.

(22) Holstein, T. Studies of Polaron Motion Part 2. The “Small” Polaron. *Ann. Phys. (Amsterdam, Neth.)* **1959**, *8*, 343–389.

(23) Su, W. P.; Schrieffer, J. R.; Heeger, A. J. Solitons in Polyacetylene. *Phys. Rev. Lett.* **1979**, *42* (25), 1698–1701.

(24) Dissado, L. A.; Walmsley, S. H. Exciton-Induced Lattice Distortion and Excimer Formation. *Chem. Phys.* **1984**, *86* (3), 375–387.

(25) Sumi, H. Two Kinds of Excimers in α -Perylene and Pyrene Crystals: Origin of Y and V Emissions. *Chem. Phys.* **1989**, *130* (1–3), 433–449.

(26) Zhao, Y.; Brown, D. W.; Lindenberg, K. A Variational Approach to Nonlocal Exciton–phonon Coupling. *J. Chem. Phys.* **1997**, *106* (7), 2728.

(27) Chen, D.; Ye, J.; Zhang, H.; Zhao, Y. On the Munn-Silbey Approach to Polaron Transport with off-Diagonal Coupling and Temperature-Dependent Canonical Transformations. *J. Phys. Chem. B* **2011**, *115* (18), 5312–5321.

(28) Luo, B.; Ye, J.; Guan, C.; Zhao, Y. Validity of Time-Dependent Trial States for the Holstein Polaron. *Phys. Chem. Chem. Phys.* **2010**, *12* (45), 15073–15084.

(29) Sun, J.; Luo, B.; Zhao, Y. Dynamics of a One-Dimensional Holstein Polaron with the Davydov Ansatz. *Phys. Rev. B: Condens. Matter Mater. Phys.* **2010**, *82* (1), 014305.

(30) Munn, R. W.; Silbey, R. Theory of Electronic Transport in Molecular Crystals. II. Zeroth Order States Incorporating Nonlocal Linear Electron–phonon Coupling. *J. Chem. Phys.* **1985**, *83* (4), 1843.

(31) Zhao, Y. Doctoral thesis; University of California: San Diego, 1994.

(32) Zhao, Y.; Li, G.; Sun, J.; Wang, W. An Improved Variational Approach to off-Diagonal Exciton-Phonon Coupling. *J. Chem. Phys.* **2008**, *129* (12), 124114.

(33) Liu, Q.; Zhao, Y.; Wang, W.; Kato, T. Global-Local Ansatz and Dynamical Coherent Potential Approximation Study of off-Diagonal Exciton-Phonon Coupling. *Phys. Rev. B: Condens. Matter Mater. Phys.* **2009**, *79* (16), 165105.

(34) Ku, L. C.; Trugman, S. A. Quantum Dynamics of Polaron Formation. *Phys. Rev. B: Condens. Matter Mater. Phys.* **2007**, *75* (1), 014307.

(35) Meier, T.; Zhao, Y.; Chernyak, V.; Mukamel, S. Polarons, Localization, and Excitonic Coherence in Superradiance of Biological Antenna Complexes. *J. Chem. Phys.* **1997**, *107*, 3876.

(36) Zhao, Y.; Brown, D. W.; Lindenberg, K. A Variational Approach to Nonlocal Exciton – Phonon Coupling A Variational Approach to Nonlocal Exciton – Phonon Coupling. *J. Chem. Phys.* **1997**, *106*, 2728.

(37) Zhao, Y.; Brown, D. W.; Lindenberg, K. Variational Energy Band Theory for Polarons: Mapping Polaron Structure with the Toyozawa Method Variational Energy Band Theory for Polarons: Mapping Polaron Structure with the Toyozawa Method. *J. Chem. Phys.* **1997**, *107*, 3159. Brown, D. W.; Lindenberg, K.; Zhao, Y. Variational Energy Band Theory for Polarons: Mapping Polaron Structure with the Global-Local Method. *J. Chem. Phys.* **1997**, *107* (8), 3179.

(38) Sun, J.; Duan, L.; Zhao, Y. Delocalized Davydov D1 Ansatz for the Holstein Polaron. *J. Chem. Phys.* **2013**, *138* (17), 174116.

(39) Zhou, N.; Chen, L.; Zhao, Y.; Mozyrsky, D.; Chernyak, V.; Zhao, Y. Ground-State Properties of Sub-Ohmic Spin-Boson Model with Simultaneous Diagonal and off-Diagonal Coupling. *Phys. Rev. B: Condens. Matter Mater. Phys.* **2014**, *90* (15), 155135.

(40) Dirac, P. A. M. *Math. Proc. Cambridge Philos. Soc.* **1930**, *26*, 376. Frenkel, J. *Wave Mechanics*; Oxford University Press: Oxford, U.K., 1934.

(41) Zhao, Y.; Luo, B.; Zhang, Y.; Ye, J. Dynamics of a Holstein Polaron with off-Diagonal Coupling. *J. Chem. Phys.* **2012**, *137* (8), 084113.

(42) Davydov, A.; Kislukha, N. Solitons in one-dimensional molecular chains. *JETP* **1976**, *44* (3), 571.

(43) Davydov, A. S. *Solitons in Molecular Systems*; Springer, Reidel: Dordrecht, 1985.

(44) Škrinjar, M. J.; Kapor, D. V.; Stojanović, S. D. Classical and Quantum Approach to Davydovs Soliton Theory. *Phys. Rev. A: At, Mol, Opt. Phys.* **1988**, *38* (12), 6402–6408.

(45) Förner, W. Accuracy of Davydov D₁ Approximation for Soliton Dynamics in Proteins. *Phys. Rev. B: Condens. Matter Mater. Phys.* **1996**, *53* (10), 6291–6317.

(46) Cruzeiro-Hansson, L. Two Reasons Why the Davydov Soliton May Be Thermally Stable After All. *Phys. Rev. Lett.* **1994**, *73* (21), 2927–2930.

(47) Zhou, N.; Huang, Z.; Zhu, J.; Chernyak, V.; Zhao, Y. Polaron Dynamics with a Multitude of Davydov D₂ Trial States. *J. Chem. Phys.* **2015**, *143* (1), 014113.

(48) Brixner, T.; Stenger, J.; Vaswani, H. M.; Cho, M.; Blankenship, R. E.; Fleming, G. R. Two-Dimensional Spectroscopy of Electronic Couplings in Photosynthesis. *Nature* **2005**, *434* (7033), 625–628.

(49) Engel, G. S.; Calhoun, T. R.; Read, E. L.; Ahn, T. Evidence for Wavelike Energy Transfer through Quantum Coherence in Photosynthetic Systems. *Nature* **2007**, *446*, 782.

(50) Collini, E.; Wong, C. Y.; Wilk, K. E.; Curmi, P. M. G.; Brumer, P.; Scholes, G. D. Coherently Wired Light-Harvesting in Photosynthetic Marine Algae at Ambient Temperature. *Nature* **2010**, *463* (7281), 644–647.

(51) Panitchayangkoon, G.; Hayes, D.; Fransted, K. A.; Caram, J. R.; Harel, E.; Wen, J.; Blankenship, R. E.; Engel, G. S. Long-Lived Quantum Coherence in Photosynthetic Complexes at Physiological Temperature. *Proc. Natl. Acad. Sci. U. S. A.* **2010**, *107* (29), 12766–12770.

(52) Myers, J. A.; Lewis, K. L. M.; Fuller, F. D.; Tekavec, P. F.; Yocum, C. F.; Ogilvie, J. P. Two-Dimensional Electronic Spectroscopy of the D1-D2-Cyt b559 Photosystem II Reaction Center Complex. *J. Phys. Chem. Lett.* **2010**, *1* (19), 2774–2780.

(53) Lewis, K. L. M.; Ogilvie, J. P. Probing Photosynthetic Energy and Charge Transfer with Two-Dimensional Electronic Spectroscopy. *J. Phys. Chem. Lett.* **2012**, *3* (4), 503–510.

(54) Romero, E.; Augulis, R.; Novoderezhkin, V. I.; Ferretti, M.; Thieme, J.; Zigmantas, D.; van Grondelle, R. Quantum Coherence in Photosynthesis for Efficient Solar-Energy Conversion. *Nat. Phys.* **2014**, *10* (9), 676–682.

(55) Mukamel, S. *Principles of Nonlinear Optical Spectroscopy*; Oxford University Press: New York, 1995.

(56) Huynh, T. D.; Sun, K. W.; Gelin, M.; Zhao, Y. Polaron Dynamics in Two-Dimensional Photon-Echo Spectroscopy of Molecular Rings. *J. Chem. Phys.* **2013**, *139* (10), 104103.

(57) Sun, K.-W.; Gelin, M. F.; Chernyak, V.; Zhao, Y. Davydov Ansatz as an Efficient Tool for the Simulation of Nonlinear Optical Response of Molecular Aggregates. *J. Chem. Phys.* **2015**, *142* (21), 212448.

(58) Tanimura, Y.; Kubo, R. Time Evolution of a Quantum System in Contact with a Nearly Gaussian-Markoffian Noise Bath. *J. Phys. Soc. Jpn.* **1989**, *58* (1), 101–114.

(59) Tanimura, Y. Nonperturbative Expansion Method for a Quantum System Coupled to a Harmonic-Oscillator Bath. *Phys. Rev. A: At, Mol, Opt. Phys.* **1990**, *41* (12), 6676–6687.

(60) Tanimura, Y. Stochastic Liouville, Langevin, Fokker–Planck, and Master Equation Approaches to Quantum Dissipative Systems. *J. Phys. Soc. Jpn.* **2006**, *75* (8), 082001.

(61) Ishizaki, A.; Tanimura, Y. Quantum Dynamics of System Strongly Coupled to Low-Temperature Colored Noise Bath: Reduced Hierarchy Equations Approach. *J. Phys. Soc. Jpn.* **2005**, *74* (12), 3131–3134.

(62) Chen, L.; Zhao, Y.; Tanimura, Y. Dynamics of a One-Dimensional Holstein Polaron with the Hierarchical Equations of Motion Approach. *J. Phys. Chem. Lett.* **2015**, *6* (15), 3110–3115.

(63) Chen, L.; Gelin, M. F.; Domcke, W.; Zhao, Y. Theory of Femtosecond Coherent Double-Pump Single-Molecule Spectroscopy: Application to Light Harvesting Complexes. *J. Chem. Phys.* **2015**, *142* (16), 164106.